ORIGINAL ARTICLE

Machine learning for multi-dimensional performance optimization and predictive modelling of nanopowder-mixed electric discharge machining (EDM)

Muhammad Sana[1] · Muhammad Asad[1] · Muhammad Umar Farooq[2] · Saqib Anwar[3] · Muhammad Talha[1]

Abstract

Aluminium 6061 (Al6061) is a widely used material for various industrial applications due to low density and high strength. Nevertheless, the conventional machining operations are not the best choice for the machining purposes. Therefore, amongst all the non-conventional machining operations, electric discharge machining (EDM) is opted to carry out the research due to its wide ability to cut the materials. But the high electrode wear rate (EWR) and high dimensional inaccuracy or overcut (OC) of EDM limit its usage. Consequently, nanopowder is added to the dielectric medium to address the abovementioned issues. Nanopowder mixed EDM (NPMEDM) process is a complex process in terms of performance predictability for different materials. Similarly, the interactions between the process parameters such as peak current (I_p), spark voltage (S_v), pulse on time (P_{on}) and powder concentration (C_p) in dielectric enhance the parametric sensitivity. In addition, the cryogenic treatment (CT) of electrodes makes the process complex limiting conventional simulation approaches for modelling inter-relationships. An alternative approach requires experimental exploration and systematic investigation to model EWR and overcutting problems of EDM. Thus, artificial neural networks (ANNs) are used for predictive modelling of the process which are integrated with multi-objective genetic algorithm (MOGA) for parametric optimization. The approach uses experimental data based on response surface methodology (RSM) design of experiments. Moreover, the process physics is thoroughly discussed with parametric effect analysis supported with evidence of microscopic images, scanning electron microscopy (SEM) and 3D surface topographic images. Based on multi-dimensional optimization results, the NT brass electrode showed an improvement of 65.02% in EWR and 59.73% in OC using deionized water. However, CT brass electrode showed 78.41% reduction in EWR and 67.79% improved dimensional accuracy in deionized water. In addition to that, CT brass electrode gave 27.69% less EWR and 81.40% improved OC in deionized water compared to kerosene oil.

Keywords Machine learning · Electric discharge machining · Geometric accuracy · Aluminium · Multivariate analysis

Nomenclature

Al6061	Aluminium 6061
EWR	Electrode wear rate
SR	Surface roughness
NT	Non-treated

I_p	Peak current
P_{on}	Pulse on time
RLT	Recast layer thickness
CMM	Coordinate measuring machine
ANN	Artificial neural network
SEM	Scanning electron microscopy
CCD	Central composite design
EDM	Electric discharge machining
OC	Overcut
MRR	Material removal rate
CT	Cryogenic treatment
C_p	Powder concentration
S_v	Spark voltage
ANOVA	Analysis of variance
R^2	Coefficient of determination

✉ Muhammad Umar Farooq
  mn21muf@leeds.ac.uk; Umarmuf0@gmail.com

1. Department of Industrial and Manufacturing Engineering, Faculty of Mechanical Engineering, University of Engineering and Technology, Lahore 54890, Pakistan

2. School of Mechanical Engineering, University of Leeds, Leeds LS2 9JT, UK

3. Industrial Engineering Department, College of Engineering, King Saud University, P.O. Box 800, 11421 Riyadh, Saudi Arabia

RSM   Response surface methodology
MOGA   Multi-objective optimization genetic algorithm

1 Introduction

Aluminium alloys, particularly Al6061, has great popularity in the field of aircraft, marine, automotive and medical sectors. Such an extensive prominence of aforementioned Al alloy is due to its phenomenal characteristics including low density, high electro-thermal conductivities, superb formability, excellent malleability and non-corrosive nature [1, 2]. However, machining of said alloy is really troublesome when conventional processes are used because it prone to chips adhesion and edge deformation. This can result in high surface roughness (SR), electrode wear rate (EWR) and overcut (OC) [3–5]. SR evaluates the surface quality and EWR defines the electrode wear per unit time, while OC justifies the proper dimensional accuracy. Therefore, a non-conventional technique, such as EDM, has been selected for the cutting of Al 6061. EDM die sinker is a stochastic process that is applied to cut electrically conductive materials [6, 7]. Irrespective of taking the mechanical features, EDM can develop intricate geometry with precise tolerances and reproducibility [3, 8–10]. The fundamental principle of die sinker EDM revolves around eroding material from the specimen by means of repetitive electric sparks that are generated in the region of electrode (usually acts as cathode) and workpiece (usually acts as anode) [7, 11]. At first, high-voltage pulses are produced by a power supply. When the voltage reaches a certain threshold, the dielectric fluid breaks down and spark occurs between the two conductive surfaces, vaporizing a trace amount of material from both specimen and electrode. The removed debris are then resolidified over the machined cavity by a dielectric fluid [12]. Conventionally, kerosene oil is engaged as dielectric medium, but it emits hazardous gases, vapours and fumes which cannot only affect the human health but also disturb the environment [13]. This happens due to inherent properties of kerosene oil, such as high flammability, greater toxicity, non-biodegradability and low viscosity [14]. Different studies have been found on the issues associated with the kerosene oil. For example, Ming et al. [15] studied that EDM under kerosene oil releases toxic fumes and aerosol products which simultaneously affect the operator's health and air quality. Thus, kerosene oil is not conductive for attaining sustainable and green EDM. Tonshoff et al. [16] mentioned that hydrocarbon-based dielectric (kerosene oil) gives harmful substances, i.e. aliphatic hydrocarbons, benzene, aerosol, dust and volatile particles. Moreover, excessive break down of kerosene oil yields carbon particles which adhere to the surface of electrode, causing hindrance in the normal discharge process. A similar findings have been reported by

Singh et al. [17], Sivapirakasam et al. [18], Radu et al. [19] and Dhakar et al. [20] Keeping in view the consequences of kerosene oil, deionized water has been utilized in this article for the EDM of Al 6061.

Although EDM offers many benefits, however its use for the fabrication of Al6061 is curtailed due to low MRR, EWR, poor surface finish and high geometric OC [21]. The solution to the given problem has been put forward by researchers, suggesting to mix nanopowder in the dielectric oil [22, 23]. The role of nanopowder in the dielectric oil plays a very crucial role for improving the said responses. The nano-additives available in the dielectric medium generate a large number of ionized particles upon the application of high voltage. These particles are accelerated and move randomly, causing dispersion in the electric discharges and widening the work-electrode distance. The increased distance leads to a bridging phenomenon, where the current's path meshes, resulting in a stable machining operation. As an outcome, machining rate is augmented [24, 25]. In the current study, alumina (Al_2O_3) nanopowder has been utilized in the deionized water while EDM of Al 6061. Despite the significance of PMEDM, it is not without its drawbacks, as it can lead to agglomeration and suspension in the dielectric medium, resulting in arcing and loss of process stability. To address this problem, researchers have recommended the addition of a surfactant [26]. Therefore, this study probed the impact of different process parameters on EWR and OC using a surfactant (Span 20)-powder mixed dielectric during the EDM of Al 6061. The aforementioned responses have great importance in terms of deciding the process performance. Such as EWR is essential to justify the dimensional accuracy and surface finish of the machined object, whereas OC is principally needed to ensure the accurate functionality of the end product. For instance, Chaudhari et al. [27] optimized the machining parameters during PMEDM of nitinol shape memory alloy (SMA). The authors used Al_2O_3 powder with the EDM oil. Three input variables, namely, pulse-on time (P_{on}), pulse-off time (P_{off}) and C_p, were considered to examine MRR, SR and RLT. A particular multi-objective teaching-learning-based optimization (TLBO) was applied to find the single feasible solution. They found significant improvement in the values of performance variables due to the presence of Al_2O_3 powder in the EDM oil. Hosni and Lajis [28] assayed the effect of chromium (Cr) C_p and surfactant (Span-20) concentration (C_s) on AISI D2 steel by employing response surface methodology (RSM) during EDM process. The authors revealed that C_p was the most contributing factor in terms of improving the MRR, EWR and SR output parameters. They also noticed that optimal values for both C_p and C_s were 2.155 g/l and 10.000 g/l, respectively. In the context of EDM process, Abbas et al. [29] utilized the same workpiece material, surfactant and powder as stated in the previous study. They selected copper

as the electrode material to examine the SR of AISI D2 steel against three factors: C_p, C_s and P_{on}. A comparative assessment was conducted between the findings of C_p and C_s. The study demonstrated that higher C_p and T_{on} values significantly reduce the SR as compared to the behaviour of C_s. The researchers obtained the minimum SR under optimal settings of C_p (2 g/l) and T_{on} (20 μs).

Kolli and Kumar [30] proposed surfactant and graphite powder-assisted EDM for titanium alloy. Analysis was performed on dielectric fluid behaviour, MRR, SR, RLT, surface topology and energy-dispersive X-ray spectroscopy. They claimed that addition of surfactant (Span-20) not only improved the responses by reducing abnormal sparks but also minimize the agglomerated particles and suspension in the dielectric medium. Paswan et al. [31] conducted a study to investigate the effect of deionized water mixed with graphene nanopowder on the machining performance of Inconel 718 during EDM. The study examined the MRR, SR and TWR of the material in relation to three design parameters: I_p, P_{on} and gap voltage (V_g). The researchers used RSM to optimize the machine variable settings based on these parameters and also conducted waveform analysis to examine the spark phenomena. The results indicated a significant improvement in the magnitude of responses, with values of MRR, TWR and SR improving by 20.1%, 2% and 14%, respectively. Moreover, the waveform analysis demonstrated that the discharge was more stable in the nanographene mixed dielectric as compared to conventional EDM. The study conducted by Rouniyar and Shandilya [32] investigates OC in magnetic field assisted powder mixed (MFAPM)-EDM of Al 6061 alloy to enhance the process stability. Al powder was mixed with EDM oil as the dielectric. Process parameters such as discharge current (DC), C_p, P_{on}, P_{off} and magnetic field strength were varied during experimentation using Box-Behnken design. A semi-empirical model was formulated using dimensional analysis to predict OC and found better than the RSM model. Optimum process parameters for minimal OC were determined using the desirability function approach of RSM, and DC was found to be the most important one. Confirmatory experiments showed good correlation between optimal and experimental outcomes. The investigators sought to examine the standalone performance of powder type, surfactant type and CT effects on various workpiece surfaces during the machining process. The appraisal of EDM's effectiveness is determined by the influence of CT on the electrodes. It has been noted that the introduction of CT to the electrodes induces an enhancement in grain structure, consequently improving responses such as thermal and electrical conductivities of the electrode [33].

Utilizing CT stands out as a recognized method to enhance electrode conductivity, marking a hallmark of material refinement. This process contributes to the improvement of material properties such as hardness, toughness, grain size, thermal conductivity and electrical conductivity. The underlying rationale for these improvements is linked to the contraction of material microstructures when exposed to liquid nitrogen at -184 °C for a specified duration. Subsequently, a reverse process, tempering, is executed, leading to an increase in the aforementioned material properties [34, 35]. An investigation by Ozdemir [36] revealed that the shallow CT at -84 °C resulted in improved hardness, wear and toughness properties of high Fe-Cr steel. The author further concluded that shallow CT also positively influenced the microstructure. In a study by Senthilkumar and Rajendran [37] on En 19 steel, shallow CT demonstrated a 114% increase in wear characteristics compared to the untreated material. Choudhary et al. [38] employed Taguchi's L18 orthogonal array with CT and NT copper electrode on Hastelloy C-4 as the EDM base material. They studied SR and EWR concerning input parameters like spark duration, current and gap voltage. The findings indicated that cryo-treated copper electrodes exhibited lower EWR and superior SR compared to untreated ones. EDM machining efficiency was investigated by Thanigaivelan et al. [39] using cryogenically treated copper, brass electrodes and simple brass electrodes. The study revealed a 24% improvement in EWR and a 2.5% enhancement in OC value by adjusting the input parameters with CT electrodes. Papazoglou et al. [7] determined the cutting ability of EDM in the machining of Ti alloy grade 2 in a dielectric medium. The authors concluded that MRR was largely influenced by I_p, and EWR was impacted by the spark-on time during the EDM machining process.

Teimouri and Baseri [40] reported about magnetic field assisted EDM performance in terms of EWR and OC by employing rotary electrode. They conducted experiments under three different regimes: (i) low energy, (ii) middle energy and (iii) high energy. Three input parameters, namely, current, rotational speed of electrode, P_{on} and P_{off}, were taken into account. They found that EWR upsurges with the increase in current and tool rotational speed. However, for the high energy regime, minimum EWR has been achieved due to protective layer of carbon over the tool surface. Kumar and Sharma [41] also conducted their research on magnetic field assisted EDM of EN-31 for assessing the three responses, namely, MRR, EWR and OC. Likewise previous study, current, P_{on} and P_{off} were taken as input parameters. Their research concluded that maximum MRR and minimum TWR and OC were found when P_{on}, P_{off}, current and magnetic field set at 10 μs, 10 μs, 3.18 A and 0.3 T, respectively. Rashedul et al. [42] discussed the impact of various electrodes, namely, Ti-alloy (TC4), stainless steel (SS304), Cu-W alloys (W70Cu30, W80Cu20, W90Cu10) and brass, on the electrochemical discharge machining (ECDM) performance. They examined MRR, EWR and OC. Amongst all the mentioned electrodes, researchers obtained the better results of MRR, EWR and OC with the

Cu-W electrode (W70Cu30). This was happened because of its high thermal conductivity than rest of the electrodes. Meena et al. [43] performed multi-response optimization by grey relational analysis (GRA) for the EDM of commercially pure (CP) Ti-alloy. The MRR, EWR and OC were calculated against three input parameters (current, frequency and pulse width). They declared current as most affecting parameter. The GRA suggested that values of MRR, EWR and OC are 0.006495 mm³/min, 0.005959 mm³/min and 0.048 mm, at optimized parametric setting (frequency = 125 kHz, current = 35 A and pulse width = 1 µs), respectively. Ramaswamy and Perumal [44] machined hybrid composite LM13 Al alloy to optimize the machining parameters through EDM setup. They varied current, P_{on} and P_{off} for the evaluation of MRR, EWR and OC. After applying ANOVA, researchers found that current and P_{on} are most contributing factors for MRR, EWR and OC, respectively. The desirability function of RSM technique was applied for the optimization of conflicting parameters. They noted that, at parameter setting of current (19.99 A), P_{on} (4.85 µs) and P_{off} (7.99 µs), 1.2830 mm³/s, 0.3441 mm/s and 0.0607 mm values were recorded for MRR, EWR and OC, respectively.

After a thorough literature review, it has been observed that there is extensive research on surfactant and PMEDM of various alloys. However, the effect of NT and CT brass electrodes with Span-20 and alumina blend with deionized water has not yet been investigated for Al6061 alloy. Therefore, the main objective of this study is to analyse the machine learning assisted PMEDM with four multivarious input factors—I_p, S_v, P_{on} and C_p(s)—on EWR and OC by using a mixture of Span-20 and Al_2O_3 nano-additives in deionized water during EDM of selected Al alloy with NT and CT brass electrode. The findings have been explained by incorporating the microscopic, SEM and 3D profilometry images. ANOVA has also been conducted to find out the significant input parameters which directly influenced the EWR and OC for both the NT and the CT brass electrodes. An ANN has also been constructed to predict the magnitudes of response measures. Moreover, a comparison of experimental, RSM and ANN predicted values of EWR and OC has also been made for both the NT and CT brass electrodes for the selected Al6061 material during the machining process. In addition to that, a MOGA has also been performed for the optimal settings of input parameters where the best response measures have been achieved. However, a comparison has also been built for the deionized water and conventional dielectric (kerosene) for sustainable EDM.

2 Materials and methods

The workpiece material chosen for assessing the cutting performance of the mentioned Al alloy was Al6061. The cutting performance of Al6061 was evaluated by measuring the EWR and the degree of dimensional inaccuracy. To serve as a dielectric fluid, deionized water was used in a specialized container. The chemical composition of Al6061 was analysed using spectrometry and is listed in Table 1; however, the physical properties are presented in Table 2 [45]. The workpiece has the dimensions of 60 mm × 60 mm × 5 mm.

To evaluate the cutting performance, brass with a diameter of 9 mm was employed as the electrode against Al6061 alloy, both in NT and deep CT conditions. The physical and electrical properties of the brass electrode can be found in Table 3 [46]. The deep cryogenic treatment was carried out in a cryogenic chamber, where the brass electrode was subjected to a temperature of − 184 °C at the rate of 1 °C/min in liquid nitrogen for 24 h. After the cooling procedure in the cryogenic chamber, the electrode was subjected to tempering of 150 °C at the same rate at which cooling was performed

Table 1 Chemical composition of Al6061

Element	Wt. %
Al	95.85–98.56
Mg	0.8–1.2
Si	0.4–0.8
Cu	0.15–0.4
Pb	0.05
Ti	0.15
Zn	0.25
Fe	0.7
Cr	0.04–0.35
Ni	0.05
Sn	0.05
Mn	0.15

Table 2 Physical and electrical properties of Al6061

Sr. no	Property	Value
1	Density (g/mm³)	0.0027
2	Electrical resistivity (Ω·m)	4×10^{-8}
3	Melting point (°C)	5.2×10^{6}
4	Specific heat capacity (J/g °C)	0.89
5	Thermal conductivity (W/mK)	1.66×10^{2}

Table 3 Physical properties of the brass electrode

Properties (units)	Value
Density (g/mm³)	8.55×10^{-3}
Electrical resistivity (Ω·m)	4.7×10^{-7}
Melting point (°C)	990
Specific heat capacity (J/g °C)	0.380
Electrical conductivity (S/m)	16×10^{6}

Table 4 Levels of input parameters

Parametric levels	I_p (A)	S_v (V)	P_{on} (μs)	C_p (g/100 ml)
1	5	2	50	0.5
2	15	4	100	1.0
3	15	6	150	1.5

Table 5 Electrical and physical properties of alumina powder

Sr. no	Properties (unit)	Value
1	Density (g/cm³)	0.97
2	Electrical resistivity (μΩm)	14.2×10^{-2}
3	Melting point (°C)	2045
4	Thermal expansion (K⁻¹)	2.81×10^{-3}
5	Thermal conductivity (W/mK)	35

(1 °C/min). At the end, the electrode was cooled at the room temperature. Later the deep CT, the grain size of the brass electrode was improved by up to 7.89%, whereas the conductivity improved by 10.70% [47]. In order to address the limitations of low cutting rates in EDM, three different concentrations (0.5, 1, 1.5 g/100 ml) of alumina (Al_2O_3) were added to the deionized water, based on preliminary trials and a literature review. The parametric levels used in this study are presented in Table 4, while the physical and chemical properties of alumina nanopowder are outlined in Table 5 [48]. In order to avoid the agglomeration during the EDM process, a fixed concentration (6% by volume) of Span-20 was utilized.

The experimental design employed in this study utilized a RSM approach known as the CCD. The experimentation was carried out using the EDM (Model RJ: 230) machine, as depicted in Fig. 1. The EWR (mm³/min) was determined by measuring the weight difference before and after the EDM process and calculating it using Eq. 1. On the other hand, the OC was measured using a CMM and computed using Eq. 2.

$$EWR = \frac{W_B - W_A}{t_m} \tag{1}$$

$$OC = \frac{D_{cavity} - D_{tool}}{2} \tag{2}$$

where W_A and W_B are the weights of the electrode before and after the machining, respectively, though, t_m shows the machining time. However, in Eq. 2, D_{cavity} and D_{tool} are the diameters of machined profiles and the electrode, respectively.

The illustration outlining the OC is presented in Fig. 2. To determine the most effective parametric configurations for achieving minimal EWR and OC, preliminary experiments were conducted. Parameters that exhibited less EWR and greater dimensional accuracy in these initial trials were chosen for the final workpiece experimentation involving both NT and CT electrodes. The selection of these definitive parameters not only contributed to less EWR and high dimensional accuracy but also minimized the risk of overprocessing costs or tool and workpiece burning during EDM operations. Another vital step involved determining the surfactant content in the deionized dielectric. While an initial reference was obtained from the literature, the ultimate decision was based on preliminary experimental tests aligned
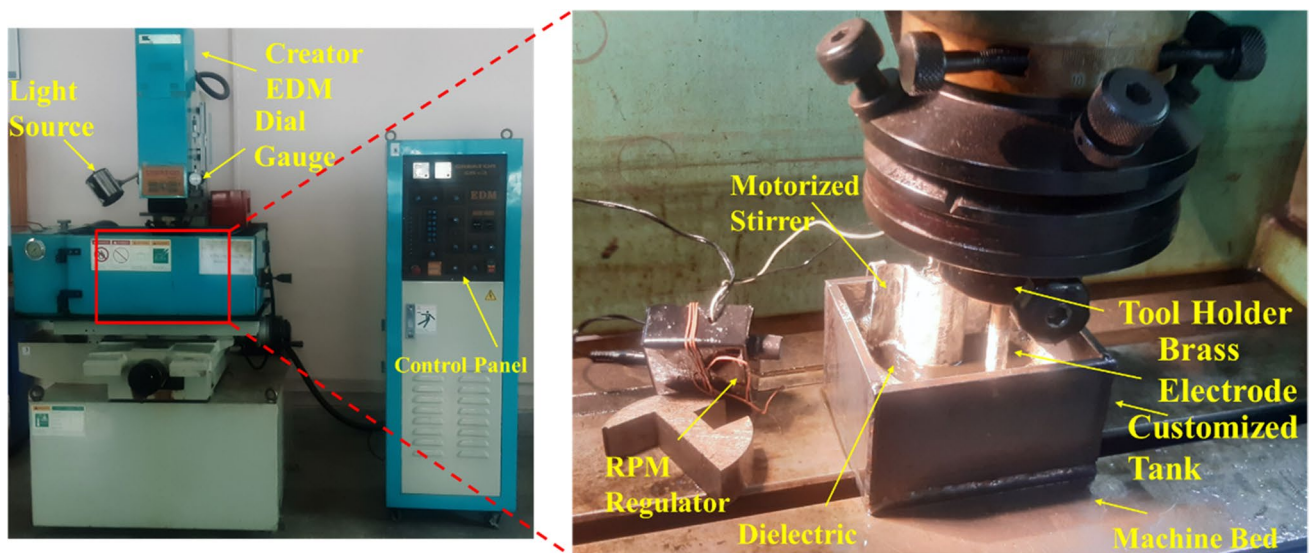
Fig. 1 Working of EDM
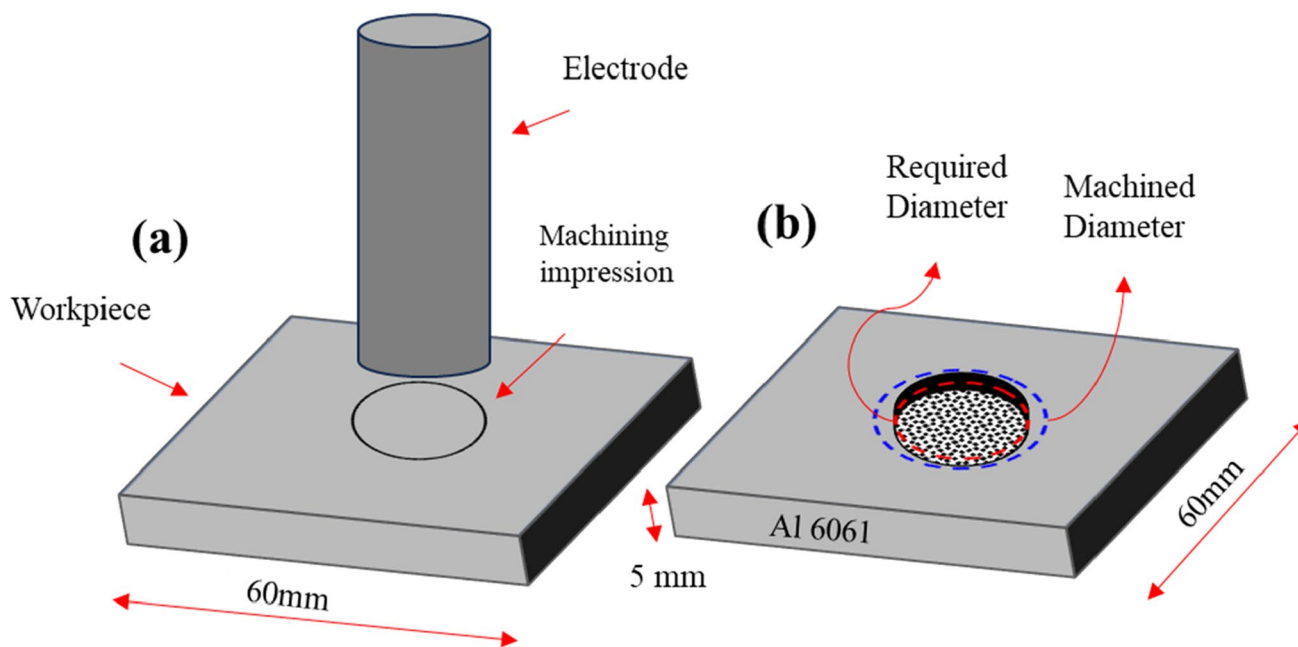
Fig. 2 Schematic for dimensional inaccuracy or OC

with the specified selection criteria. Initial results suggest that a surfactant concentration of 6% meets the requirements. A motorized stirrer tank was engineered to blend the surfactant and deionized water dielectric. The complete methodology of this study is illustrated in Fig. 3.

3 Results and discussion

Table 6 presents the experimental results of the machining process involving Al6061 alloy with both non-treated and CT brass electrodes, focusing on the measurements of EWR and OC. The findings and discussions are supported by the utilization of 3D surface plots, microscopic images and SEM analysis. Additionally, statistical significance analysis, ANN modelling for response prediction and MOGA were carried out.

3.1 Parametric effect analysis

The analysis of parametric effects was conducted to examine the influence of NT and CT brass electrodes on the EWR and dimensional inaccuracy (OC) in the EDM of Al6061. The effects of varying process parameters (I_p, S_v, P_{on} and C_p) on the response variables were investigated using 3D surface plots. It is important to note that the 3D surface plots illustrate the impact of two parameters within their specified ranges, while the remaining parameters are kept at their mid-levels.

3.1.1 Electrode wear rate

The EWR was evaluated under various process parameters using both NT and CT brass electrodes in the EDM of Al6061. Figure 4a illustrates the EWR determination using the NT brass electrode with the process parameters I_p and S_v. As shown in Fig. 4a, an increase in I_p and S_v led to an increase in EWR. This can be attributed to the higher spark density at higher I_p and S_v values, causing some of the discharge heat to melt and vaporize the electrode material. However, when the CT brass electrode was used during the machining process, a reduction in EWR was observed across all levels of process parameters, as shown in Fig. 4b, compared to the NT electrode. CT offers the significant advantage of improving the wear characteristics of the electrode [36]. This improvement can be attributed to the enhanced grain size and atom packing resulting from CT, which ultimately leads to improve wear properties and a decrease in EWR.

Figure 4c presents the surface plot depicting the relationship between the EWR and the process parameters I_p and P_{on}. It can be observed that both I_p and P_{on} have a direct impact on the EWR. An increase in the magnitude of these process parameters leads to the generation of higher discharge heat for a longer duration, causing some of the discharge energy to melt and vaporize the electrode material. However, when the CT brass electrode is utilized in the EDM of Al6061, the wear properties are improved, resulting in lesser erosion of the electrode material, as shown in Fig. 4d. One of the main reasons for the reduction in EWR is the increase in thermal
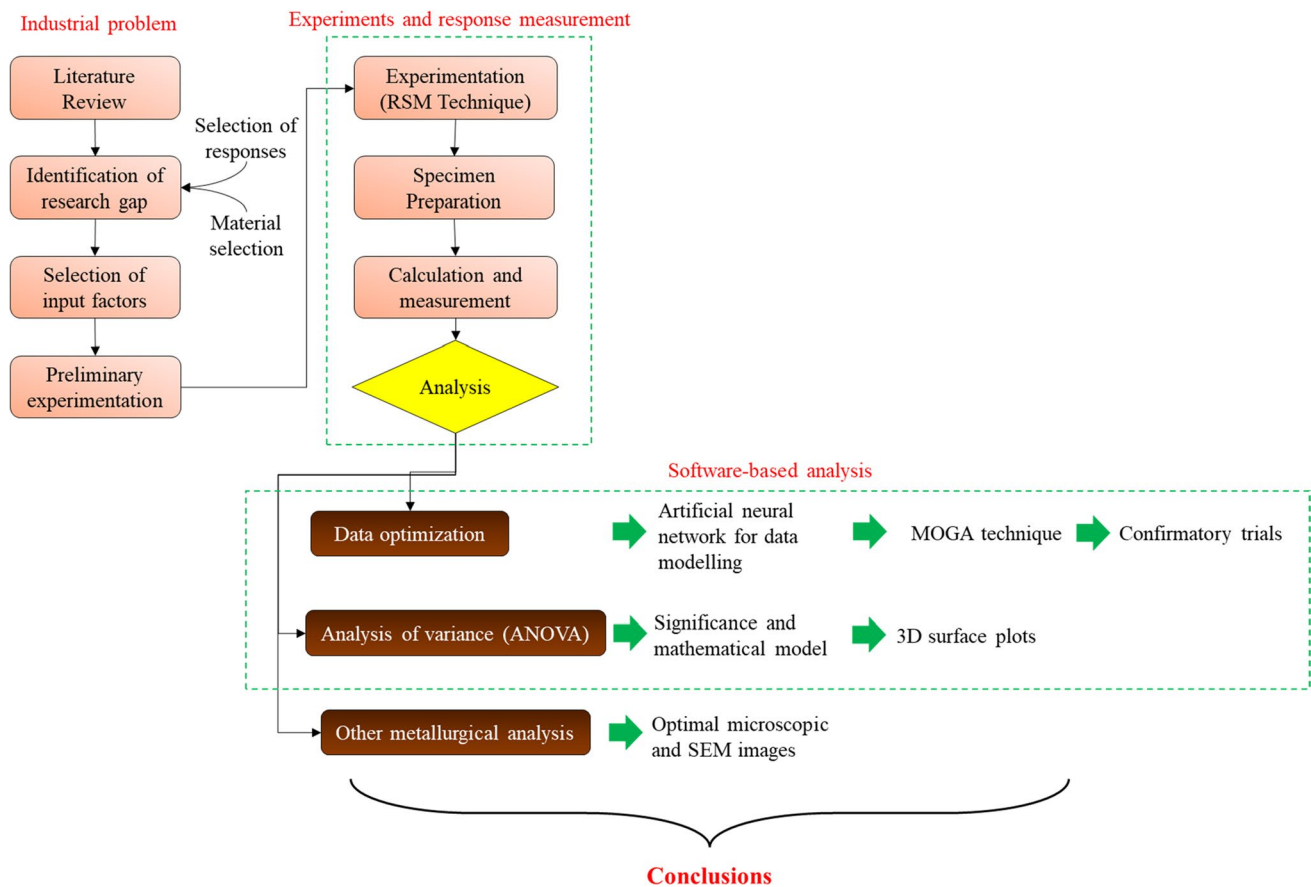
Fig. 3 Research methodology of this study

Table 6 Experimental results of response measures

	Machining responses			
	Non-treated brass		Treated brass	
	EWR	OC	EWR	OC
	mm³/min	mm	mm³/min	mm
Mean	8.27	0.18	6.44	0.15
Median	8.23	0.18	6.235	0.16
Std. Dev	2.22	0.04	2.29	0.04
Minimum	3.67	0.09	1.62	0.04
Maximum	12.11	0.26	10.11	0.24

conductivity of the electrode due to CT, in accordance with the Wiedemann-Franz-Lorenz law. The enhanced thermal conductivity facilitates rapid heat transfer from the electrode to the workpiece material, thereby reducing the EWR [47].

The EWR was also assessed by varying the levels of I_p and C_p of Al_2O_3, as depicted in Fig. 4e and f, for the EDM of Al6061 using both NT and CT brass electrodes. Figure 4e shows that an increase in the magnitude of I_p leads to high EWR. However, alumina concentration up to an optimal level (1 g/100 ml) results in an increase in EWR, but after that a depreciation was found in the magnitude of EWR. This is due to the fact that the highest C_p formed agglomeration, due to which no heat energy transfer to brass electrode and hence, a drop was recorded in EWR. However, when the CT brass electrode is used instead of the NT brass electrode, a decrease in EWR is observed at every level of process parameters (I_p and P_c), as shown in Fig. 4f. This decrease can be attributed to the improved wear characteristics of the CT brass electrode. The CT enhances the thermal conductivity of the brass electrode, leading to improved heat dissipation and reduced heat trapping in the electrode. As a result, the EWR decreases [49, 50].

3.1.2 Overcut

Figure 5a illustrates the impact of I_p and S_v on the OC during the machining of Al6061 using the NT brass electrode. It can be observed that an increase in either I_p or S_v leads to an increase in OC. This is because the higher discharge heat generated during the spark causes an increase in OC. Figure 6a–d provide a schematic representation of the generation of plasma channels at different magnitudes of I_p and
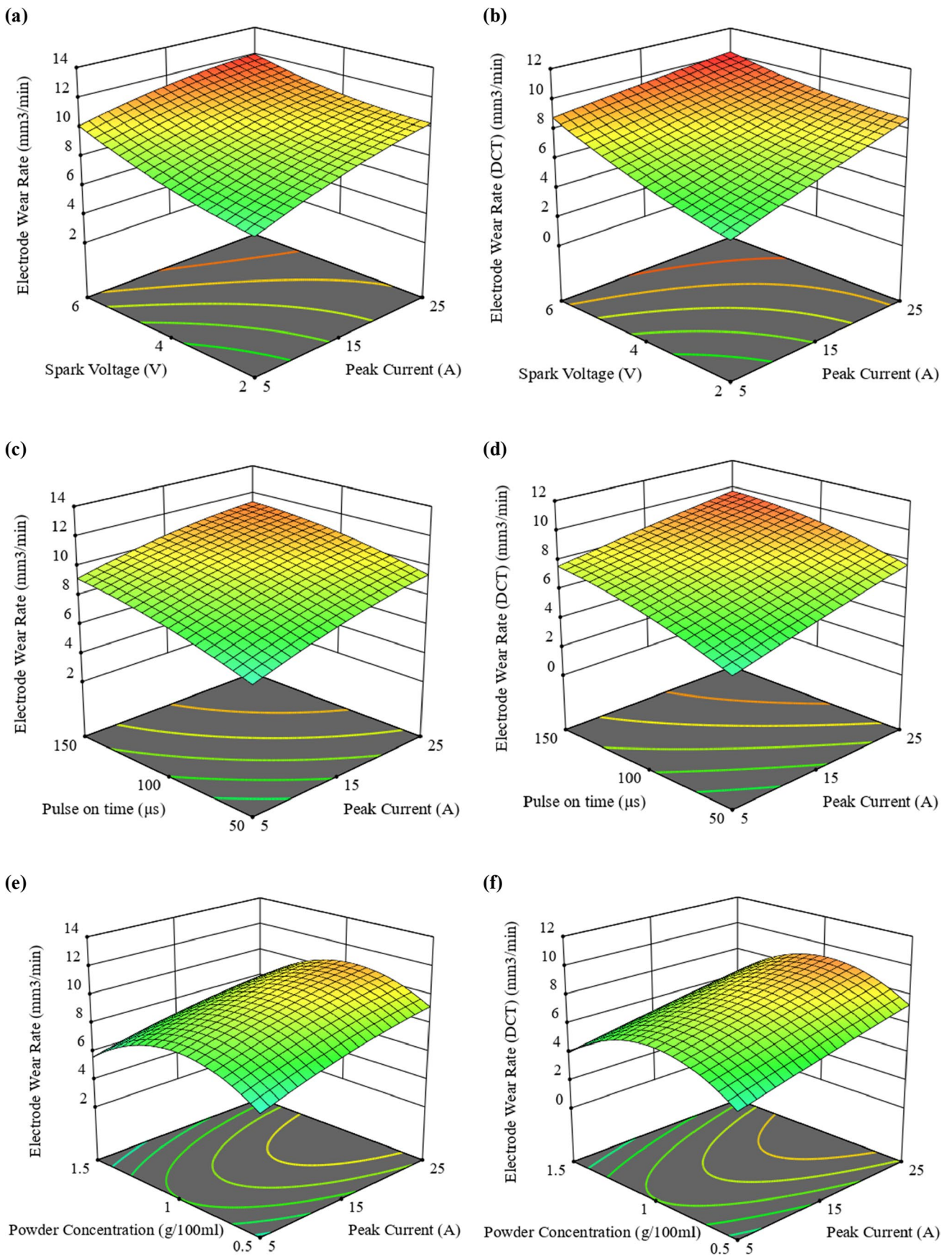
◄**Fig. 4** The 3D surface plots of EWR at different processing parameters using **a**, **c**, **e** NT brass electrode; **b**, **d**, **f** DCT brass electrode

S_v. At lower values of these process parameters, as shown in Fig. 6a, the width of the plasma channel is narrower compared to Fig. 6b. However, as the values of I_p and S_v increase, the width of the plasma channel also increases. The increase in plasma channel width leads to a higher discharge heat during the EDM process, resulting in the melting and vaporization of the workpiece material, thus causing a higher OC. On the other hand, when the CT brass electrode is used with Al6061, regular sparking is observed even at high values of the input parameters. This leads to a reduction in OC compared to the NT electrode, as the regular sparking prevents excessive material melting and vaporization, resulting in a decreased OC.

Figure 5c presents the evaluation of OC by varying the levels of I_p and P_{on} during the EDM of Al6061 using the NT brass electrode. It can be observed from Fig. 5c that an increase in the magnitude of I_p and P_{on} leads to an increase in OC. This is attributed to the higher magnitude of process parameters, which results in an increased plasma channel, as depicted in Fig. 6a–d. However, when the CT brass electrode is utilized for the machining of Al6061 in the presence of deionized water, Fig. 5d shows a decrease in OC compared to the NT brass electrode shown in Fig. 5c. The improved performance of the CT brass electrode can be attributed to the reduction in grain size and the prevention of irregular sparking, resulting in a more controlled and precise machining process, hence leading to a decreased OC.

The OC was examined with various input parameters (I_p and C_p) using both the NT and CT brass electrode during the machining of Al6061 in the presence of deionized water. Figure 5e demonstrates that an increase in I_p leads to an increase in OC, while the addition of alumina up to a concentration of 1.0 g/100 ml increases OC, but a decline is observed thereafter. This can be attributed to agglomeration occurring beyond the optimal concentration of alumina, which hinders the widening of the plasma channel, resulting in a decrease in OC at higher alumina C_ps. However, when the CT brass electrode is used instead of the NT brass electrode, Fig. 5f illustrates a decrease in OC compared to Fig. 5e. This is because the spark density generated by the CT brass electrode is more uniform in comparison to the NT brass electrode. The grain size refinement achieved through CT facilitates regular and consistent sparking, leading to improved dimensional accuracy and a decrease in OC.

3.2 Surface topographic analysis

Surface topographic analysis has been investigated for EWR and OC in the EDM process of Al6061. This analysis was conducted using both NT and CT brass electrodes. The effects of variations in input parameters (I_p, S_v, P_{on} and C_p) on the output variables have been examined through microscopic and SEM images. Additionally, 3D surfaces profilometry images have been included to assess the surface texture of the machined profiles.

3.2.1 Overcut

The diametric error for EDMed surface has been presented in Fig. 7a and b due to NT and CT brass electrodes. The NT brass electrode gave the highest OC magnitude due to irregular and uneven sparking. However, if the CT brass electrode has been engaged, then OC magnitude has been reduced due to grain size refinement of brass electrode as presented in Fig. 7b. In order to further explore the diametric error profiles, SEMs have been performed to study the recast layer. Thereof, if a NT brass electrode engaged for the machining purposes of Al6061, then it gave the highest melts redeposited during the sparking phenomenon. This is due to the fact that the irregular and uneven spark did not expel the debris properly from the workpiece surface and hence during the pulse off duration these debris redeposited on the workpiece surface and results in the increase of OC as shown in Fig. 8a. However, when CT brass electrode was engaged then due to grain size refinement, regular and even sparking expelled the debris in more refined way and results in better dimensional accuracy as shown in Fig. 8b.

3.2.2 Electrode wear rate

Figure 9a displays a microscopic image revealing shallow and small craters on the machined profile of an NT brass electrode when process parameters are set at small magnitudes. The 3D surface topography of the machined specimen demonstrates small-heightened peaks and valleys, indicating a low EWR. This low EWR can be attributed to the use of low process parameter values, resulting in a low-intensity spark density that only partially melts the brass electrode. Since the surface of the workpiece reflects the electrode, SEM analysis of the machined specimen (Fig. 10a) confirms the presence of shallow and small craters. Conversely, when the NT brass electrode is employed to machine Al6061 at higher process parameter magnitudes, deep and wide craters are formed on the machined surface as shown in Fig. 9b. The 3D surface topography exhibits heightened peaks and valleys compared to those observed at low process parameter magnitudes. The formation of these deep and wide craters is attributed to the generation of a wider plasma channel. SEM analysis performed shown in Fig. 10b under high process parameter magnitudes reveals the presence of deep and wider craters on the surface of Al6061. It can be inferred that these deep craters are also present on the surface of the brass electrode due to the high intensity of the plasma channel.
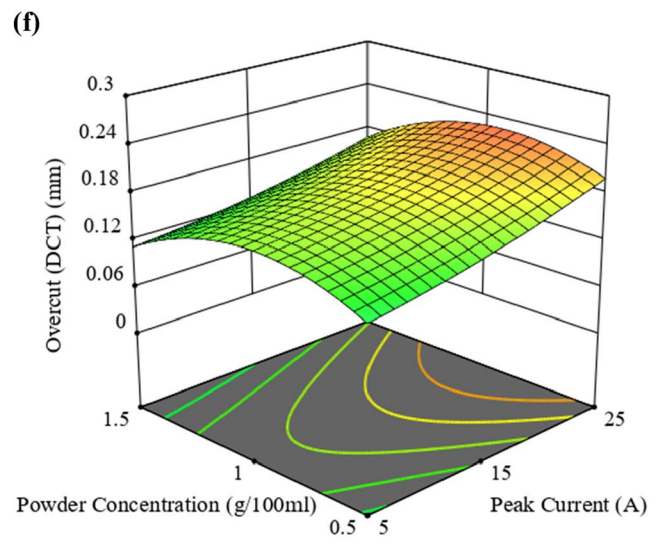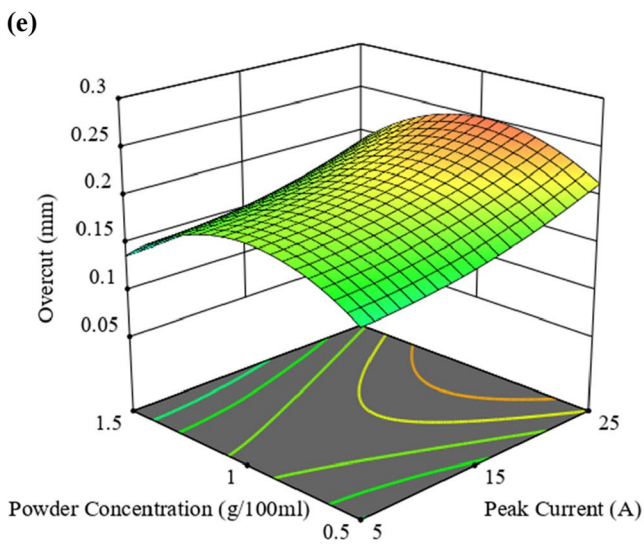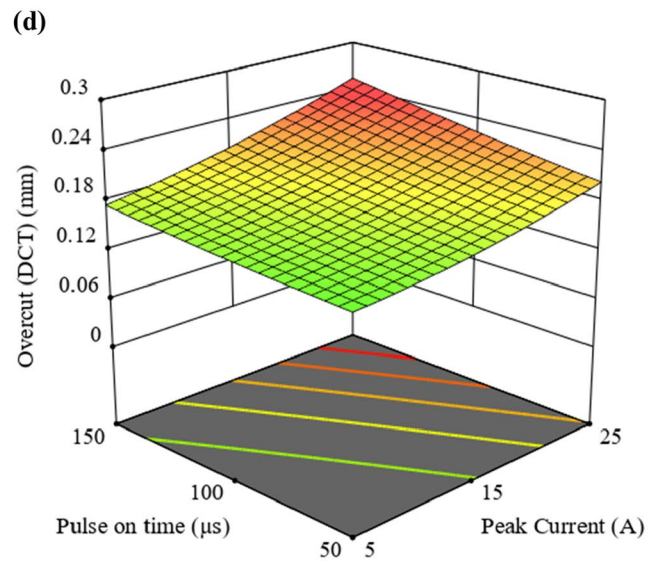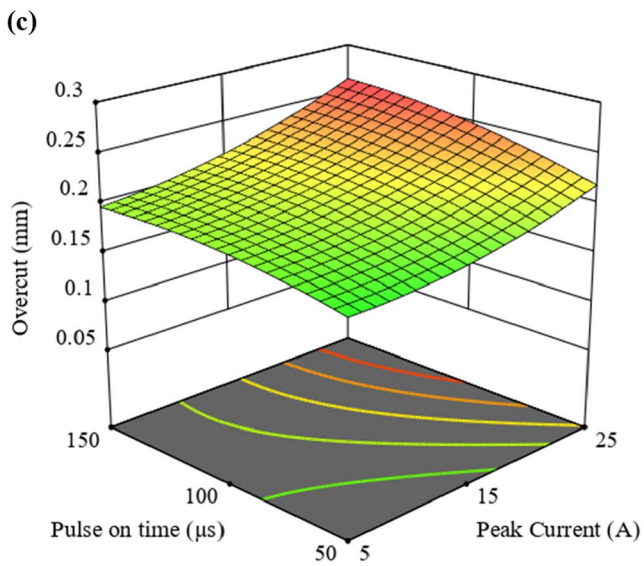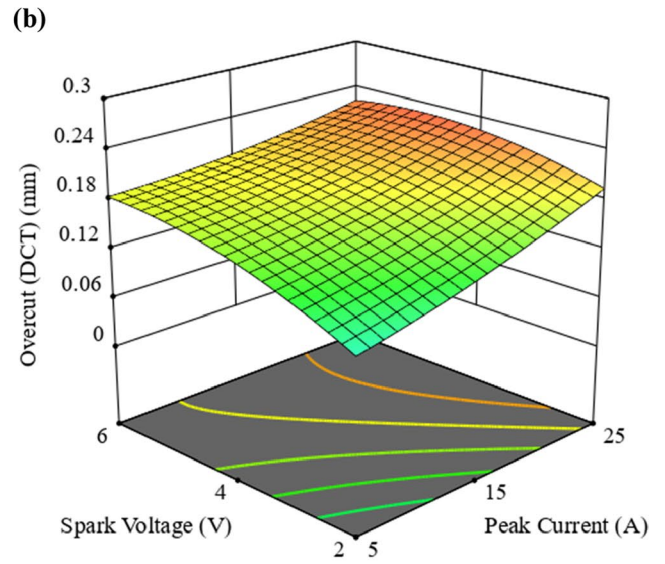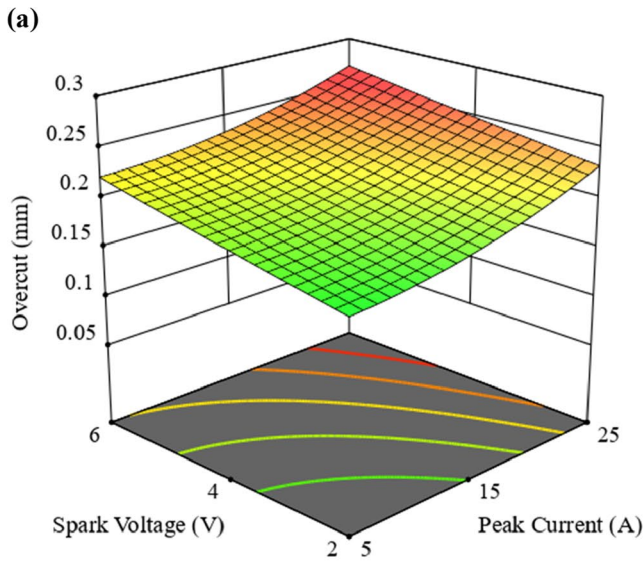
◄**Fig. 5** The 3D surface plots of OC at different processing parameters using **a**, **c**, **e** NT brass electrode; **b**, **d**, **f** DCT brass electrode

The utilization of a CT brass electrode leads to a reduction in EWR even at low process parameter magnitudes. Figure 11a displays a microscopic image depicting shallow and small craters on the brass electrode's surface, indicating minimal erosion of the electrode material. Additionally, the 3D surface topographic view reveals short-heightened peaks and valleys, signifying improved surface generation and a smaller heat-affected zone. The decrease in EWR for the brass electrode can be attributed to the increased thermal conductivity resulting from CT. This treatment prevents the trapping of heat generated during the spark and facilitates its immediate transfer to the workpiece. The rapid heat transfer from the electrode to the base material contributes to the reduced EWR. To examine the surface of machined Al6061, SEM analysis was performed on the Al alloy (Fig. 12a) machined at low process parameters. Shallow and small craters are observed on the machined specimen, and these craters are smaller in comparison to those created by the NT brass electrode. On the other hand, when the CT brass electrode is employed against the base material at high process parameter magnitudes, shallow and wide craters form on the brass electrode's surface (Fig. 11b). The shallow craters indicate minimal material erosion from the electrode. The 3D surface topographic view demonstrates short-heightened peaks and valleys, albeit smaller in comparison to those formed when using the NT brass electrode for machining Al6061. The reduced EWR can be attributed to CT, which enhances the thermal conductivity of the brass electrode, prevents heat from getting trapped within the electrode and promotes rapid heat transfer to the base material. At high process parameter magnitudes, SEM analysis (Fig. 12b) reveals deeper and smaller craters on the surface of Al6061, further supporting the notion that the CT brass electrode generates smaller craters.

3.3 Parametric significance analysis

The adequacy of the generated models was assessed using the ANOVA technique. ANOVA was employed to evaluate the statistical significance and examine the effects of process parameters and their interactions on each individual response. The significance of the parameters was determined by analysing their p values, while the percentage contribution was determined based on the F values. By comparing the R^2, adjusted R^2 and predicted R^2 values, ANOVA was used to determine the statistical adequacy of the produced models.

3.3.1 Electrode wear rate

Table 7 presents the ANOVA results for EWR_{NT} and EWR_{DCT}, obtained by utilizing the NT and CT brass electrodes, respectively. For EWR_{NT}, all main effect input parameters exhibit p values lower than 0.05, indicating their significance as model terms. Additionally, the parametric interaction of $S_v \times P_{on}$ is also found to be significant. Furthermore, the quadratic effect (C_p^2) demonstrates a p value below 0.05, indicating its significant parametric nature. As for EWR_{DCT}, the main input parameters I_p^2, S_v^2 and P_{on}^2 are significant, while the p values for the interaction combinations $I_p \times S_v$ and $S_v \times P_{on}$ are also below 0.05, suggesting their significance as model terms. Similar to EWR_{NT}, the quadratic effect (C_p^2) remains significant for EWR_{DCT}. The adequacy measures R^2 for both response measures exceed 0.9, indicating a high level of reliability. Moreover, the S/N ratios of 13.9073 and 14.6646 signify an adequate signal, allowing the empirical models to be employed for predicting EWR_{NT} and EWR_{DCT} values using Eqs. 3 and 4, respectively.

$$
\begin{aligned}
EWR_{NT} = &-6.68368 + 0.369211 \times I_p - 0.439430 \times S_v \\
&+ 0.045741 \times P_{on} + 19.01242 \times C_p - 0.017000 \times I_p \\
&\times S_v - 0.000388 \times I_p \times P_{on} - 0.039750 \times I_p \\
&\times C_p + 0.005600 \times S_v \times P_{on} - 0.077500 \\
&\times S_v \times C_p - 0.010850 \times P_{on} \times C_p - 0.003157 \times I_p^2 \\
&+ 0.101075 \times S_v^2 - 0.000142 \times P_{on}^2 - 9.02281 \times C_p^2
\end{aligned}
\tag{3}
$$

$$
\begin{aligned}
EWR_{DCT} = &-9.85804 + 0.333678 \times I_p - 0.100986 \times S_v \\
&+ 0.049863 \times P_{on} + 19.59620 \times C_p - 0.027781 \\
&\times I_p \times S_v - 0.000466 \times I_p \times P_{on} - 0.028875 \\
&\times I_p \times C_p + 0.005994 \times S_v \times P_{on} - 0.131875 \\
&\times S_v \times C_p - 0.008375 \times P_{on} \times C_p - 0.000585 \\
&\times I_p^2 + 0.089123 \times S_v^2 - 0.000167 \times P_{on}^2 \\
&- 9.27404 \times C_p^2
\end{aligned}
\tag{4}
$$

3.3.2 Overcut

Table 8 displays the results of the ANOVA performed using an NT and CT brass electrode for OC_{NT} and OC_{DCT} within the specified range of input variables. For OC_{NT}, all main effect parameters exhibit p values below 0.05, indicating their significance as terms in the model. Additionally, the p values for interaction combinations such as $S_v \times P_{on}$, $S_v \times C_p$ and $P_{on} \times C_p$ are also below 0.05, indicating their significance as model terms. The quadratic effect (C_p^2) is also found to be a significant model term. In the case of OC_{DCT}, all main effect parameters, interaction effects ($I_p \times S_v$, $S_v \times P_{on}$
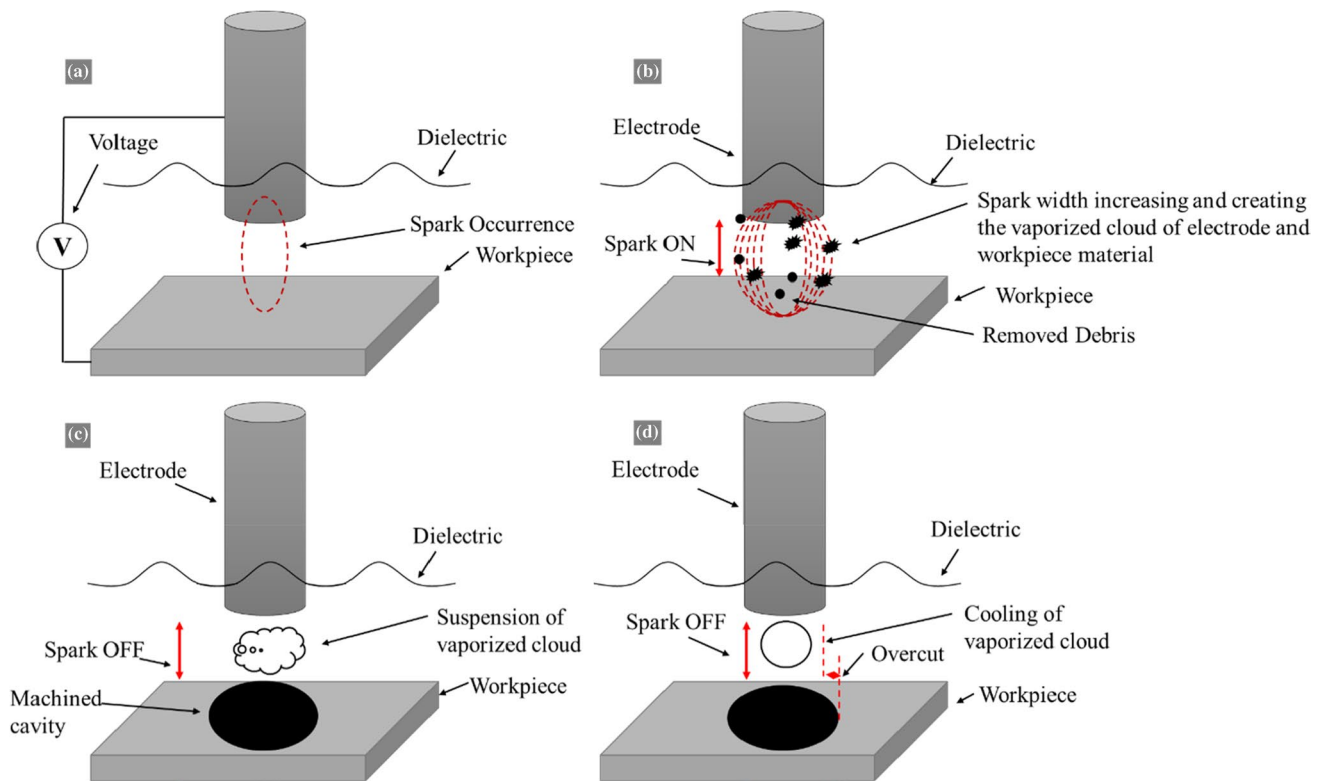
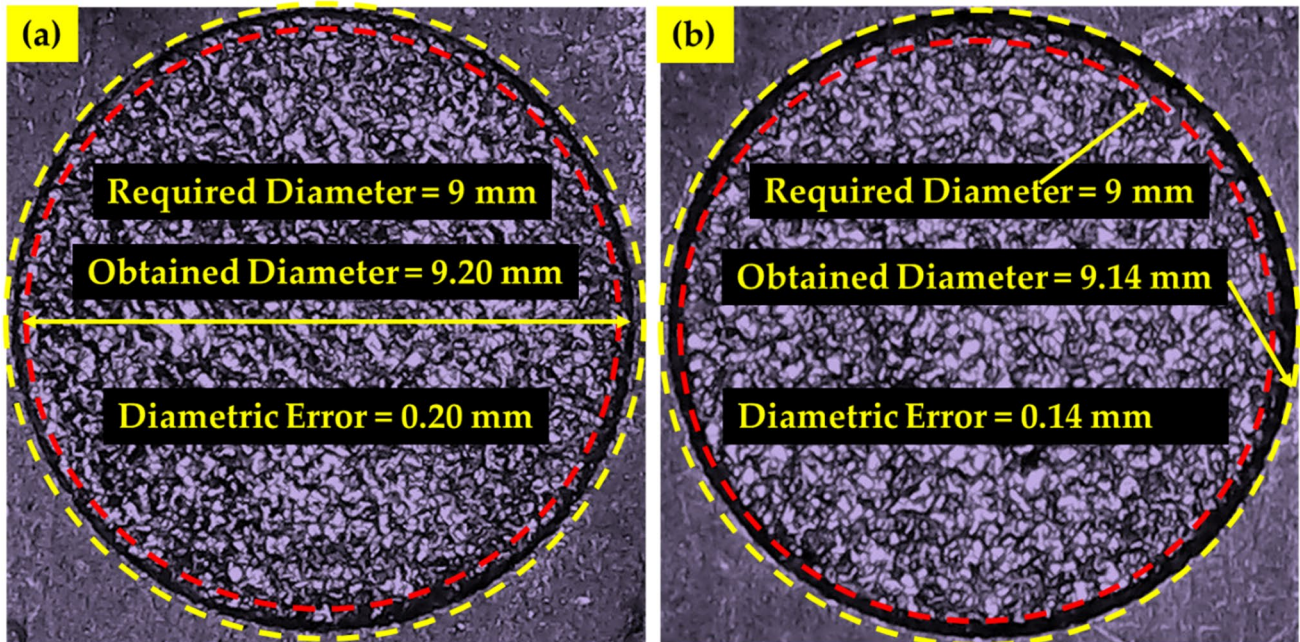**Fig. 6** Schematic of plasma generation and OC

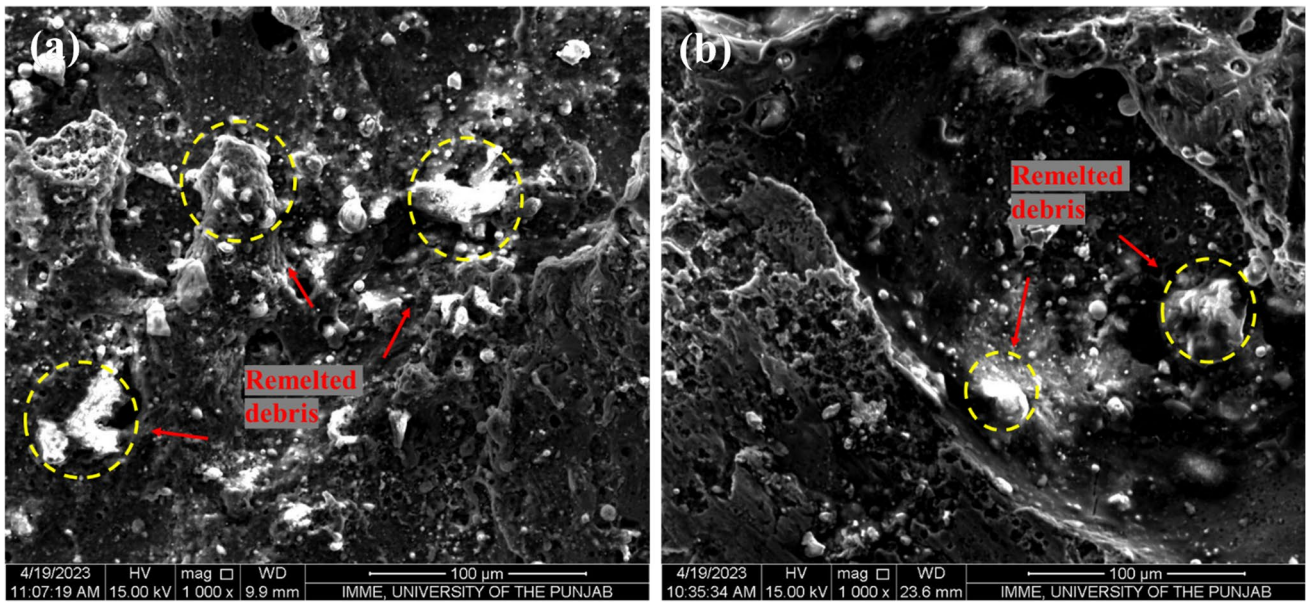**Fig. 7** Diametric error of machined profiles using **a** NT brass electrode; **b** DCT brass electrode

Fig. 8 Recast layer of melted debris on workpiece using **a** NT brass electrode; **b** DCT brass electrode
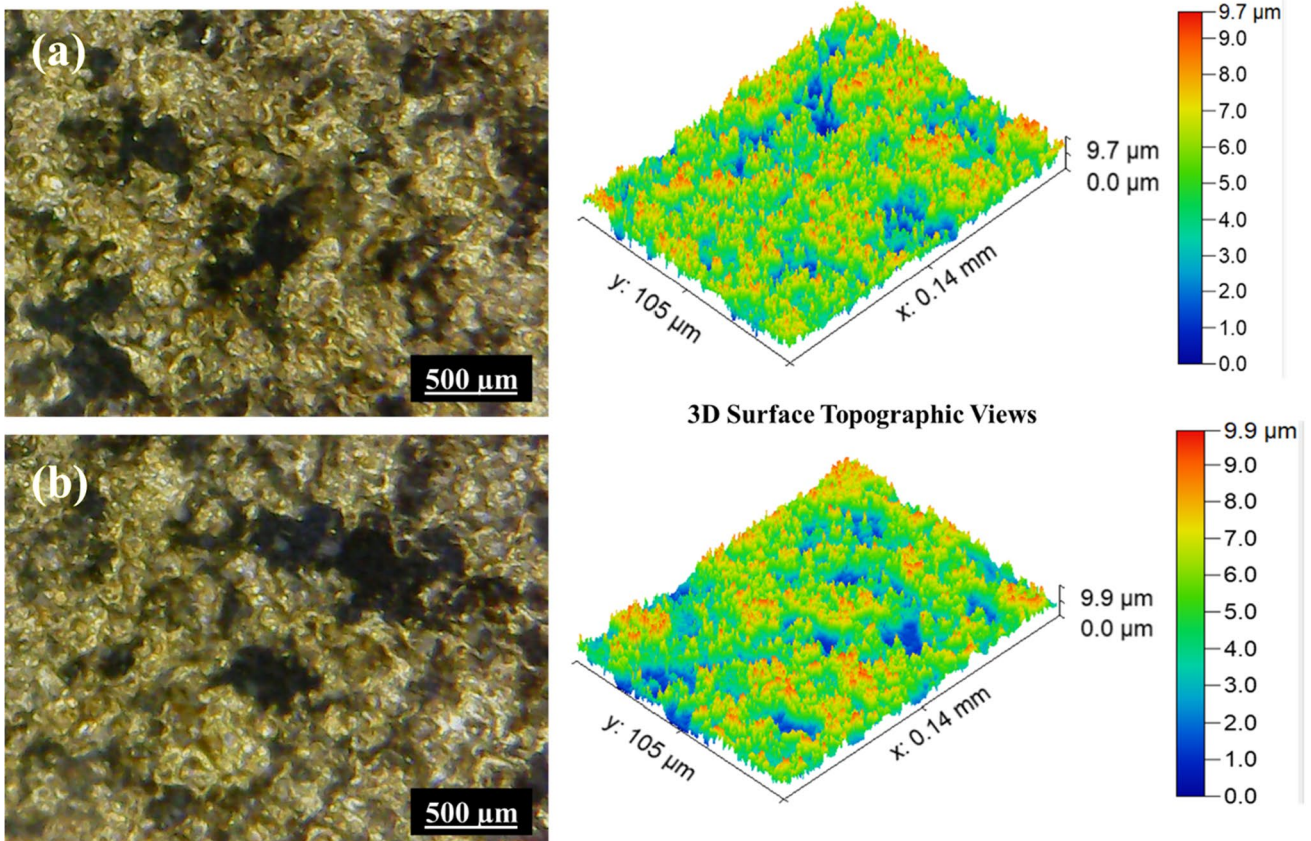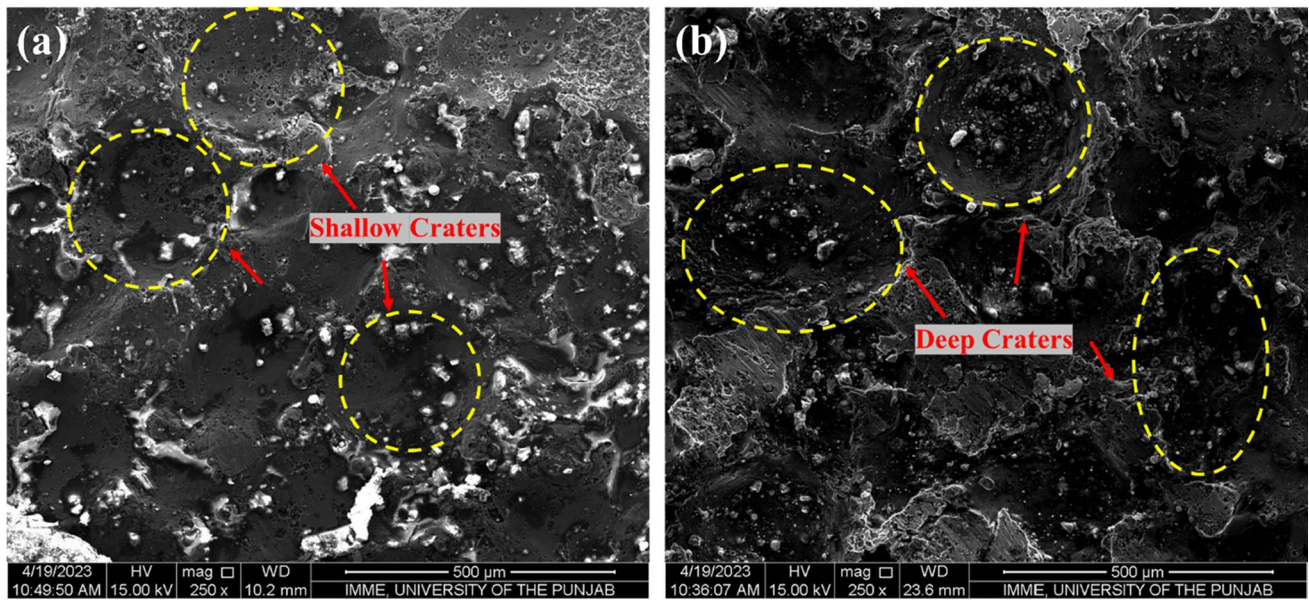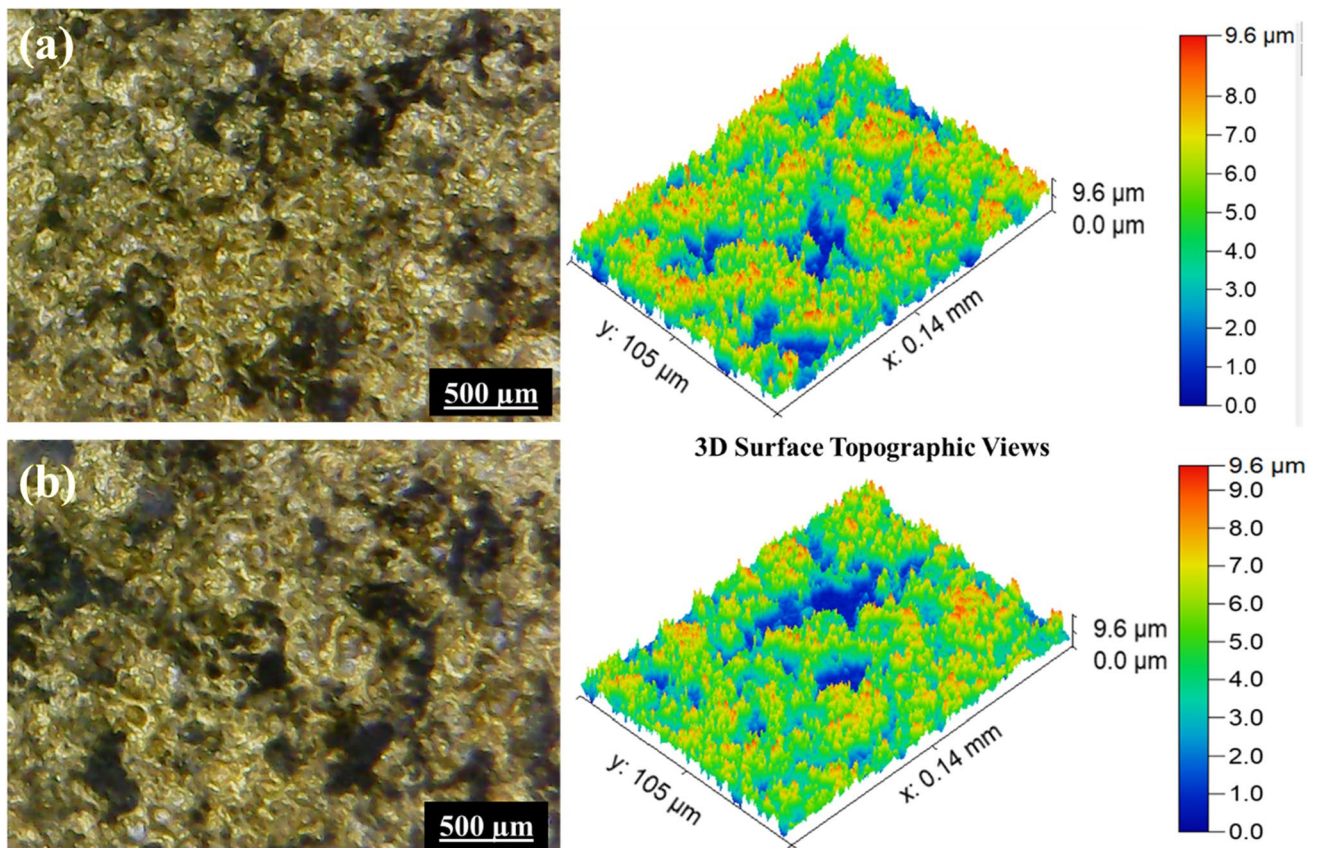

Fig. 9 Micrographs of machined NT brass electrode at **a** small magnitudes of process parameters; **b** high magnitudes of process parameters

Fig. 10 SEM of machined specimen for EWR_{NT} at **a** small magnitudes of process parameters; **b** high magnitudes of process parameters

Fig. 11 Micrographs of machined DCT brass electrode at **a** small magnitudes of process parameters; **b** high magnitudes of process parameters
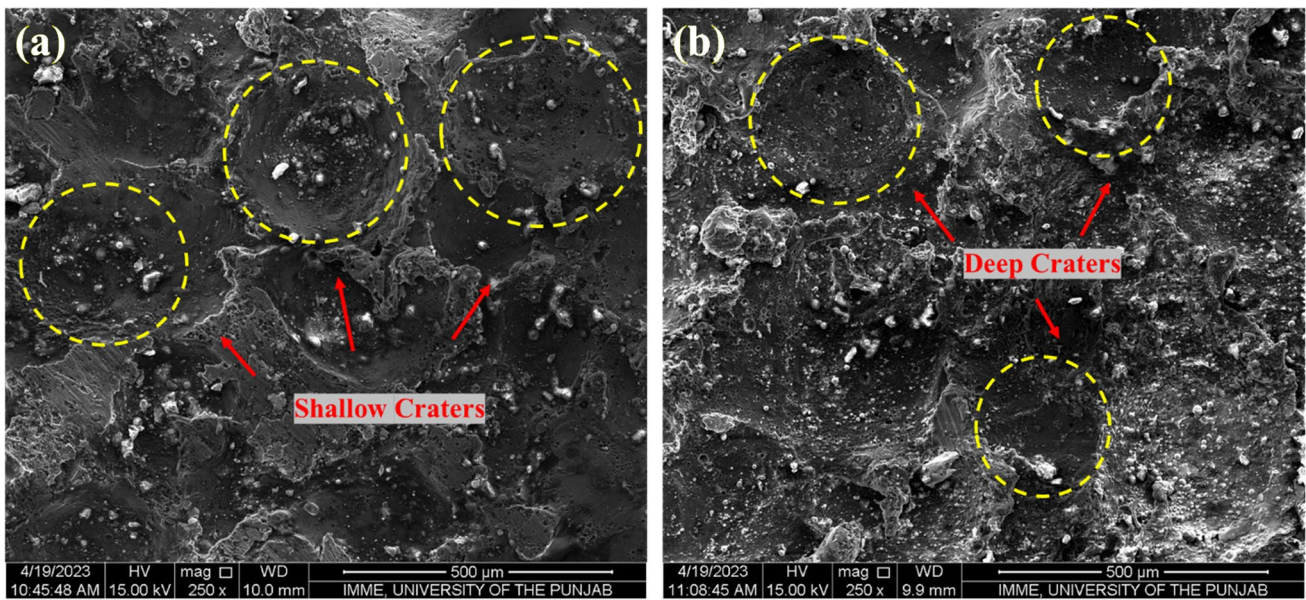
Fig. 12 SEM of machined specimen for EWR_{DCT} at **a** small magnitudes of process parameters; **b** high magnitudes of process parameters

Table 7 ANOVA for EWR_{NT} and EWR_{DCT}

EWR_{NT}				EWR_{DCT}			
Source		F value	p value	Source		F value	p value
Model		13.60	<0.0001	Model		14.94	<0.0001
I_p		40.96	<0.0001	I_p		42.77	<0.0001
S_v		35.61	<0.0001	S_v		44.81	<0.0001
P_{on}		33.13	<0.0001	P_{on}		39.82	<0.0001
C_p		6.56	0.0217	C_p		3.59	0.0777
$I_p \times S_v$		2.57	0.1298	$I_p \times S_v$		7.00	0.0184
$I_p \times P_{on}$		0.8343	0.3755	$I_p \times P_{on}$		1.23	0.2845
$I_p \times C_p$		0.8779	0.3636	$I_p \times C_p$		0.4726	0.5023
$S_v \times P_{on}$		6.97	0.0186	$S_v \times P_{on}$		8.14	0.0121
$S_v \times C_p$		0.1335	0.7199	$S_v \times C_p$		0.3943	0.5395
$P_{on} \times C_p$		1.64	0.2204	$P_{on} \times C_p$		0.9939	0.3346
I_p^2		0.3587	0.5582	I_p^2		0.0126	0.9122
S_v^2		0.5883	0.4550	S_v^2		0.4666	0.5050
P_{on}^2		0.4553	0.5101	P_{on}^2		0.6430	0.4351
C_p^2		18.31	0.0007	C_p^2		19.73	0.0005
Lack of fit		2.87	0.1279	Lack of fit		29.56	0.0008
Model summary							
Std. Dev	0.8485	R^2	0.9270	Std. Dev	0.8401	R^2	0.9331
Mean	8.28	Adjusted R^2	0.8589	Mean	6.44	Adjusted R^2	0.8706
C.V. %	10.25	Predicted R^2	0.7396	C.V. %	13.04	Predicted R^2	0.6888
Adequacy precision	13.9073	–	–	Adequacy precision	14.6646	–	–

and $P_{on} \times C_p$) and the quadratic effect (C_p^2) demonstrate significant model terms, as indicated by the respective p values. As presented in Table 8, the adequacy measure R^2 exceeds 0.93, signifying a high level of reliability. Moreover, the adequacy precision values of 14.9966 and 17.5218 indicate a strong signal, allowing the empirical model to be utilized for estimating the values of the selected response measures, namely, OC_{NT} and OC_{DCT}, using Eqs. 5 and 6, respectively.

Table 8 ANOVA for OC_{NT} and OC_{DCT}

OC_{NT}			OC_{DCT}		
Source	F value	p value	Source	F value	p value
Model	17.35	<0.0001	Model	20.36	<0.0001
I_p	57.39	<0.0001	I_p	73.71	<0.0001
S_v	36.36	<0.0001	S_v	52.27	<0.0001
P_{on}	20.10	0.0004	P_{on}	23.23	0.0002
C_p	8.63	0.0102	C_p	10.00	0.0064
$I_p \times S_v$	0.4302	0.5218	$I_p \times S_v$	10.21	0.0060
$I_p \times P_{on}$	2.69	0.1218	$I_p \times P_{on}$	3.68	0.0745
$I_p \times C_p$	0.1076	0.7475	$I_p \times C_p$	0.9188	0.3530
$S_v \times P_{on}$	10.76	0.0051	$S_v \times P_{on}$	8.27	0.0116
$S_v \times C_p$	6.88	0.0192	$S_v \times C_p$	3.68	0.0745
$P_{on} \times C_p$	31.09	<0.0001	$P_{on} \times C_p$	26.13	0.0001
I_p^2	1.38	0.2578	I_p^2	0.5608	0.4655
S_v^2	0.0145	0.9058	S_v^2	3.32	0.0884
P_{on}^2	0.8750	0.3644	P_{on}^2	0.0550	0.8177
C_p^2	26.61	0.0001	C_p^2	19.31	0.0005
Lack of fit	0.9527	0.5589	Lack of fit	2.00	0.2292
Model summary					
Std. Dev	0.0152	R^2 0.9418	Std. Dev	0.0156	R^2 0.9500
Mean	0.1847	Adjusted R^2 0.8876	Mean	0.1567	Adjusted R^2 0.9033
C.V. %	8.26	Predicted R^2 0.7074	C.V. %	9.99	Predicted R^2 0.7413
Adequacy precision	14.9966	– –	Adequacy precision	17.5218	– –
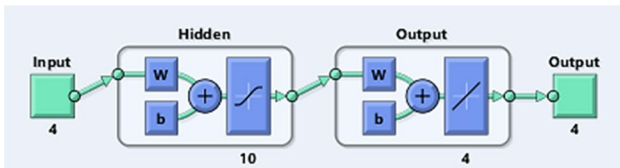
Fig. 13 Structure of present ANN study

$$OC_{NT} = -0.172098 - 0.001120 \times I_p + 0.012928 \times S_v$$
$$+ 0.002193 \times P_{on} + 0.418516 \times C_p - 0.000125$$
$$\times I_p \times S_v + 0.000012 \times I_p \times P_{on} - 0.000250$$
$$\times I_p \times C_p - 0.000125 \times S_v \times P_{on} + 0.010000$$
$$\times S_v \times C_p - 0.000850 \times P_{on} \times C_p + 0.000111$$
$$\times I_p^2 + 0.000285 \times S_v^2 - 3.54386E - 06$$
$$\times P_{on}^2 - 0.195439 \times C_p^2 \tag{5}$$

$$OC_{DCT} = -0.263363 + 0.002732 \times I_p + 0.061897 \times S_v$$
$$+ 0.001198 \times P_{on} + 0.379671 \times C_p - 0.000625$$
$$\times I_p \times S_v + 0.000015 \times I_p \times P_{on} - 0.000750$$
$$\times I_p \times C_p - 0.000113 \times S_v \times P_{on} + 0.007500$$
$$\times S_v \times C_p - 0.000800 \times P_{on} \times C_p + 0.000073$$
$$\times I_p^2 - 0.004430 \times S_v^2 + 9.12281E - 07$$
$$\times P_{on}^2 - 0.170877 \times C_p^2 \tag{6}$$

3.4 Predictive model development using machine learning

A multilayer perceptron, also known as an ANN, is a powerful tool for mapping process variables to output responses and making forecasts. This method is capable of effectively capturing complex non-linear and quadratic interactions in high-dimensional input spaces, even in systems with weakly defined relationships [51, 52]. In this study, the ANN is utilized to investigate two response measures, namely, EWR and OC, using both NT and CT brass electrodes. The ANN operates in a similar manner to the human brain, capable of performing highly non-linear tasks through the manipulation of bias and weight values. The error back propagation training algorithm (EBPTA) is employed to model the response

Fig. 14 ANN predicted EWR and OC for training, testing and validation
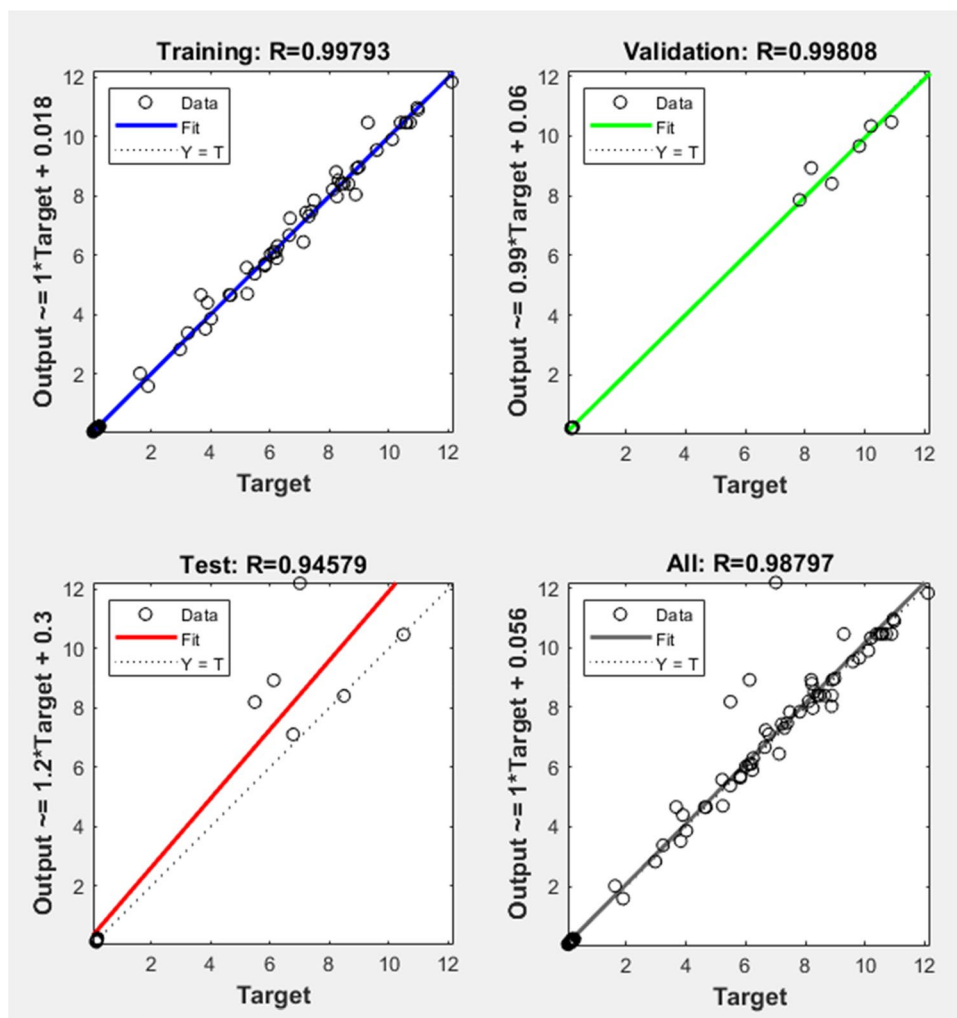
measures in this investigation [53]. Figure 13 illustrates the structure of the ANN used in the current study.

Figure 13 demonstrates the utilization of a three-layered ANN in the current study. The first layer represents the input layer, consisting of four process parameters (I_p, S_v, P_{on} and C_p). The second layer, known as the hidden layer, contains a variable number of neurons ranging from 3 to 10, selected to optimize the performance of the ANN model. By appropriately adjusting the complexity of the model's architecture, better performance and more accurate predictions along the curve can be achieved. It is important to strike a balance, as an overly complex architecture may hinder the model's ability to generalize, while too few neurons may result in poor fitting and inaccuracies across the data. Hence, the range for the ideal number of neurons is carefully chosen, typically ranging between 1 and 2.5 times the number of input variables [54]. The third and final layer is the output layer, comprising four response measures (EWR_{NT}, EWR_{DCT}, OC_{NT}

and OC_{DCT}). During the training process, 80% of the available data is used, while 10% is allocated for both testing and validation of the ANN model, respectively. Figure 14 highlights the cumulative regression coefficient R value of the ANN modelling, which is 0.98797, indicating a close relationship between the target and output values. The regression plot for the predicted ANN is also depicted. The R^2 is an essential metric for evaluating the training performance of machine learning models [55]. It quantifies the proportion of the variance in the target variable that can be explained by the model. The mathematical expression of R^2 is given as:

$$R^2 = 1 - \frac{\sum_i^N (y_i - \hat{y}_i)^2}{\sum_i^N (y_i - \bar{y}_i)^2} \tag{7}$$

Here, y_i is the actual value of output variables whereas $\hat{y}_i$ is the model-predicted value of the output variable; $\bar{y}_i$
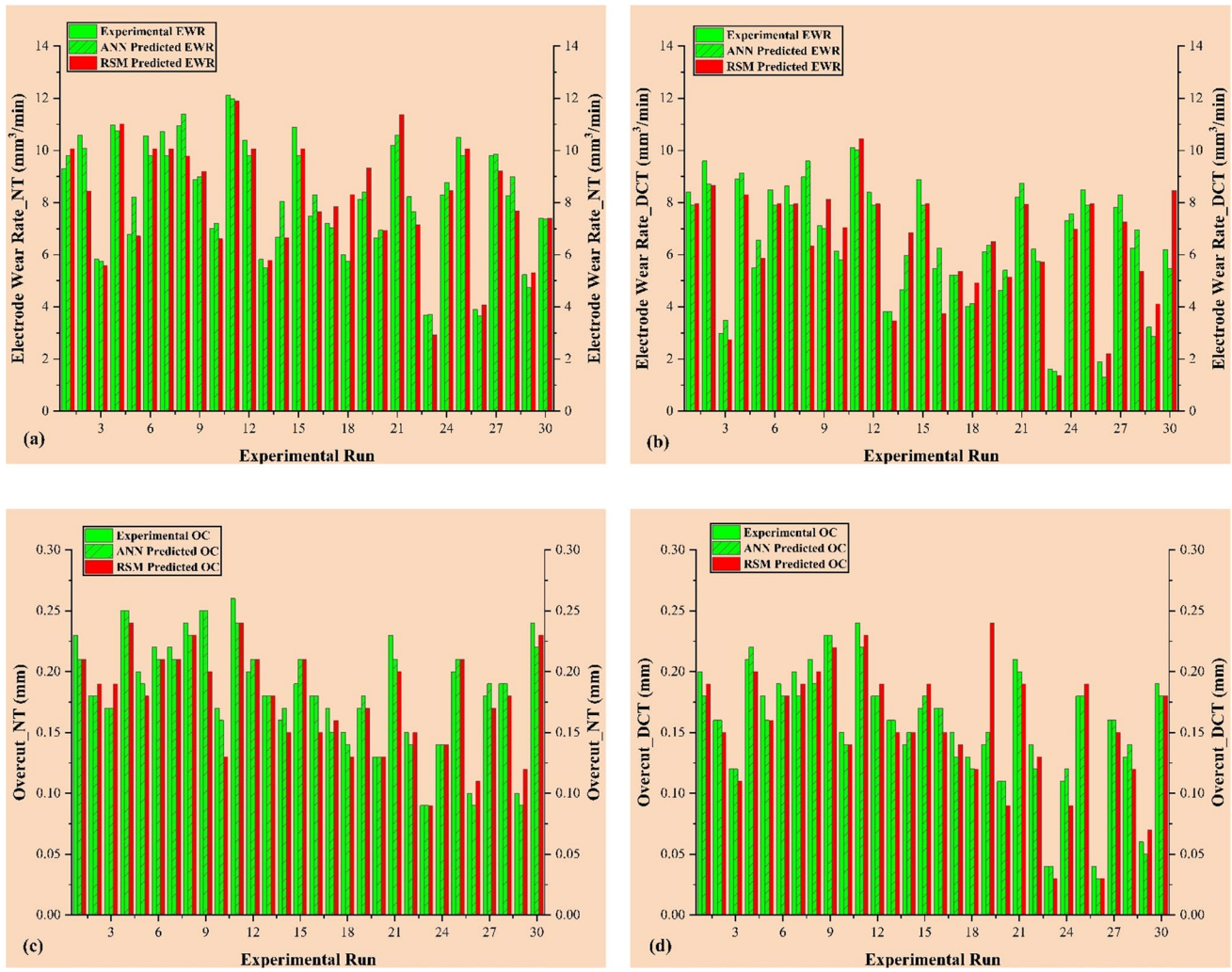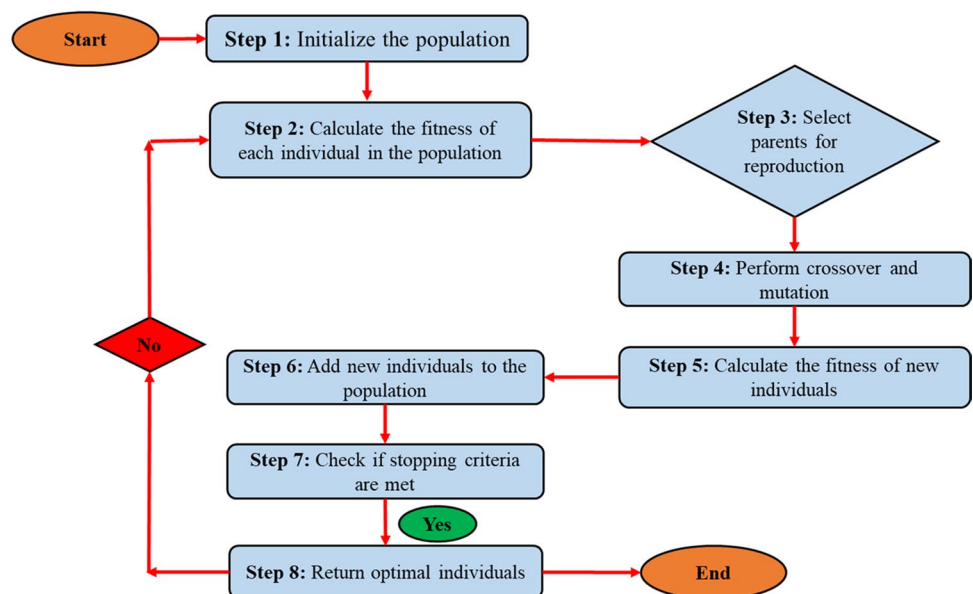
Fig. 15 Comparison of EWR and OC in experimental, ANN and RSM magnitudes using **a**, **c** NT brass electrode; **b**, **d** DCT brass electrode

Fig. 16 Working schematic of MOGA

Table 9 Optimal solutions suggested by MOGA

Sr. no	EWR_NT (mm³/min)	OC_NT (mm)	EWR_DCT (mm³/min)	OC_DCT (mm)	I_p (A)	S_v (V)	P_{on} (µs)	C_p (g/100 ml)
1	3.6690	0.1583	4.7631	0.0947	8.941	2.215	60.580	0.938
2	3.6710	0.1581	4.7405	0.0941	8.935	2.184	60.593	0.939
3	4.2485	0.1038	2.2602	0.0808	9.202	2.125	65.716	1.499
4	4.8029	0.1130	2.4706	0.0390	8.814	3.779	59.850	0.536
5	3.6742	0.1475	4.2628	0.1122	9.447	3.652	59.341	0.734
6	4.4297	0.1217	2.8927	0.0476	8.861	3.631	60.160	0.594
7	3.6700	0.1620	4.0180	0.0943	9.054	2.685	61.990	0.688
8	5.1536	0.1119	2.4370	0.0428	8.819	3.938	59.977	0.516
9	5.0079	0.1120	2.3976	0.0401	8.819	3.875	60.040	0.516
10	4.1496	0.1463	3.3855	0.0655	9.038	2.993	61.440	0.626
11	4.3262	0.1088	2.0922	0.0884	11.340	2.139	63.930	1.499
12	4.2360	0.1047	2.1825	0.0773	9.173	2.139	62.198	1.488
13	3.7758	0.1391	3.6007	0.0766	9.057	3.425	59.743	0.666
14	4.5348	0.1196	2.9876	0.0494	9.186	3.689	59.375	0.594
15	3.6690	0.1583	4.7631	0.0947	8.941	2.215	60.580	0.938
16	4.1600	0.1410	3.2362	0.0598	9.017	3.027	60.414	0.615
17	4.1490	0.1325	3.5660	0.0740	9.329	3.650	59.690	0.657
18	4.5619	0.1332	2.7185	0.0460	8.912	2.549	60.461	0.542

is the mean of y_i and $i = 1, 2, 3…, N$ equal to the total number of observations. R^2 is a measure of accuracy and varies from zero (poor prediction performance) to one (perfect degree of fit).

As it is mentioned earlier that the ANN model is used to predict the values of response measures and the R^2 in each of response measure is greater than 0.98. Herein, a comparison is developed amongst the values of response measures obtained using the experimental values and the predicted values using the ANN and RSM model as shown in Fig. 15a–d. The ANN model performed well in predicting the values of response measure in each case, i.e. EWR_{NT}, EWR_{DCT}, OC_{NT} and OC_{DCT}. Thereof, it is concluded that the ANN model is the comparatively better performing model to estimate the value of response measures.
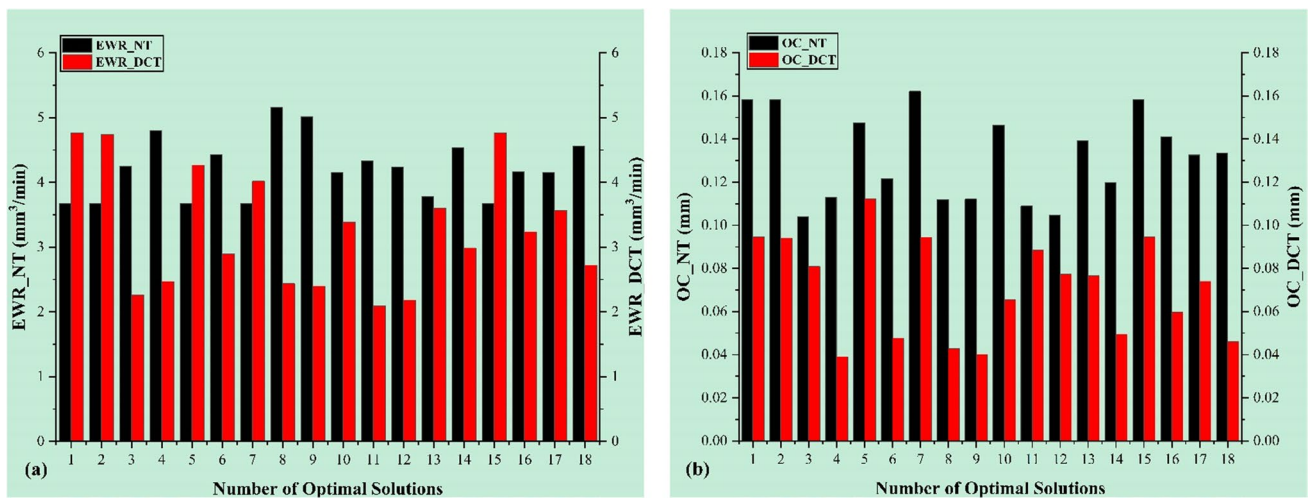
Fig. 17 Comparison of MOGA suggested optimal solutions of response measures **a** EWR; **b** OC

Table 10 Detailed information needed for confirmatory experiments

Response measures	DOE response magnitude	MOGA suggested confirmatory results	% improvement from DOE results
EWR_{NT} (mm^3/min)	12.11	4.2360	65.02%
OC_{NT} (mm)	0.26	0.1047	59.73%
EWR_{CT} (mm^3/min)	10.11	2.1825	78.41%
OC_{CT} (mm)	0.24	0.0773	67.79%

3.5 Multi-dimensional optimization through genetic algorithm

The MOGA is an evolutionary algorithm that can tackle optimization problems with multiple objectives. Since these objectives may conflict with each other, MOGA attempts to find a trade-off between them. The algorithm simultaneously searches for multiple solutions using genetic operators such as mutation and crossover. Each solution is evaluated based on its objectives, and the best solutions are selected for the next generation. The top solutions are then combined to produce even better ones, and this process is repeated until

a satisfactory solution is reached. The working schematic of MOGA is presented in Fig. 16.

In this study, MOGA is used to optimize the magnitudes of input variables for optimal solution of EWR and OC in both cases, i.e. NT and CT brass electrodes. Equation 8 highlights the objective function used to optimize the values of input variables, whereas Eq. 9 depicts the constraints for the objective function.

$$\text{Objective function} : f = \begin{cases} Minimize\ EWR \\ Minimize\ OC \end{cases} \tag{8}$$

$$\text{Constraints} : \begin{cases} 5 \le I_p \le 25 \\ 2 \le S_v \le 6 \\ 50 \le P_{on} \le 150 \\ 0.5 \le C_p \le 1.5 \end{cases} \tag{9}$$

Once MOGA is executed within the specified constraints, Table 9 indicates the multiple solutions for both input variables and output responses are successfully obtained.

The algorithm determined that to minimizing the EWR and OC, cryogenic treatment with process parameters, i.e. I_p, S_v, P_{on} and C_p values of 9.173 (A), 2.139 (V), 62.198 (μs) and 1.488 (g/100 ml), respectively, should be employed. As a result, multi-objective function suggests the EWR_{NT}

Table 11 Comparison of current findings with the existing literature

References	Alloys	EWR_NT	OC_NT	EWR_CT	OC_CT
Current study	Al6061	3.67	0.09	1.62	0.04
Bains et al. [56]	Ti-6Al-4 V	0.4260	–	–	–
Papazoglou et al. [7]	Ti-6Al-4 V Gr2	0.5350	–	–	–
Perumal et al. [57]	Ti-6242	0.0033	0.82	–	–
Choudhary et al. [58]	Ti-6Al-4 V Gr5	–	–	3.1	–
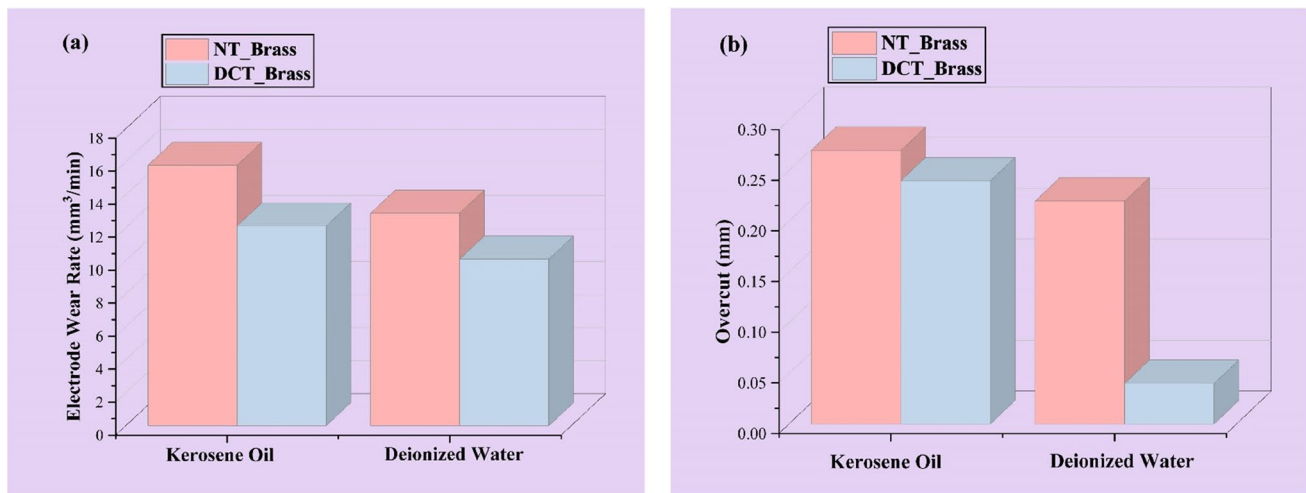
Fig. 18 Comparison of the deionized water and kerosene oil in terms of **a** EWR_{NT}, EWR_{DCT}; **b** OC_{NT}, OC_{DCT}

of 4.2360 mm³/min and 2.1825 mm³/min for EWR_{DCT}, as shown in Fig. 17a. However, the magnitudes suggested by MOGA for OC_{NT} and OC_{DCT} are 0.1047 mm and 0.0773 mm, respectively, as shown in Fig. 17b. However, the confirmatory results of response measures have been presented in Table 10.

Table 10 highlights the results for confirmatory experiments obtained using MOGA for both the EWR and OC in the case of NT and CT brass electrodes. It has been found that NT brass electrode gave 65.02% and 59.73% improvements in EWR and OC, respectively, when experimental unoptimized settings are compared with MOGA suggested values of response measures. However, significant improvements in EWR of 78.41% and OC 67.79% have been recorded, when CT brass electrode is engaged for EDM of Al6061. It is worth noting that the confirmatory results of CT brass electrode for both the EWR and OC are better than that of results NT brass electrode. However, the comparison of current study with the literature is presented in Table 11.

A comparison has been developed of EWR and OC obtained in deionized water to the conventional dielectric fluid by incorporating both the NT and CT brass electrodes as shown in Fig. 18a and b. If NT brass electrode employed to machine the Al6061, then an improvement of 30.47% in EWR and 12.5% in OC was found when deionized water used compared to kerosene oil. However, CT brass electrode gave 27.69% less EWR and 81.40% improved OC in deionized water compared to kerosene oil.

4 Conclusions

The multi-dimensional evaluation of Al6061 against different performance measures is carried out comprehensively. The experimental results have been explained with the microscopic, SEM and 3D surface topographic images. Analysis of variance was performed significant input parameters. Along with that, the machine learning is used for predictive modelling of the process. Moreover, the comparison has been built for the experimental, RSM and ANN predicted values for EWR and OC for both the NT and CT brass electrodes. Later, the multi-objective optimization through genetic algorithm has been executed for optimal parametric settings. The process science is thoroughly discussed using parametric effect analysis. After the detailed analysis, the key conclusions drawn from study are as follows:

- The minimum magnitude of EWR (1.26 mm³/min) has been obtained with the CT brass electrode which is 65.66% better than the lowest value of EWR (3.67 mm³/min) obtained by the NT brass electrode in deionized water during the EDM of Al6061. CT brass electrode showed a decrease in EWR is observed at every level of

process parameters (I_p and C_p), as compared to NT brass electrode. This decrease is mainly because of improved wear characteristics of the CT brass electrode.

- In the same way, the lowest OC (0.04 mm) magnitude has been recorded with CT brass electrode, which is 55.55% better than the lowest value of OC (0.09 mm) gained by engaging the NT brass electrode. An increase in I_p leads to an increase in OC. Similarly, the addition of alumina up to a concentration of 1.0 g/100 ml increased OC, but a decline is observed thereafter. The decline is attributed to agglomeration occurring beyond the optimal concentration of alumina, which hinders the widening of the plasma channel, resulting in a decrease in OC at higher alumina C_ps.

- Cryogenic treatment greatly impacts on the microstructure and the grain size refinement of the brass electrode. The NT brass electrode resulted in the highest OC magnitude due to irregular and uneven sparking. However, the CT brass electrode has shown that OC magnitude is significantly reduced due to grain size refinement of brass electrode.

- For OC_{NT}, all main effect parameters exhibit p values below 0.05, indicating their significance as terms in the model. In the case of OC_{DCT}, all main effect parameters, interaction effects ($I_p \times S_v$, $S_v \times P_{on}$ and $P_{on} \times C_p$) and the quadratic effect (C_p^2) demonstrate significant model terms, as indicated by the respective p values.

- The cumulative regression coefficient R value of the ANN modelling, which is 0.98797, indicates a close relationship between the target and output values.

- The multi-objective optimization through genetic algorithm has revealed that NT brass electrode gave 65.02% and 59.73% improvements in EWR and OC, respectively, when experimental unoptimized settings are compared with MOGA suggested values of response measures. However, significant improvements in EWR of 78.41% and OC 67.79% have been recorded, when CT brass electrode is engaged for EDM of Al6061.

- Based on multi-dimensional optimization results, the NT brass electrode showed an improvement of 30.47% in EWR and 12.5% in OC using deionized water as compared to kerosene oil. However, CT brass electrode showed 27.69% better or less EWR and 81.40% improved OC in deionized water compared to kerosene oil.

Author contribution Conceptualization, M.S.; methodology, M.S., M.A. and M.T.; formal analysis, M.S. and M.A.; investigation, M.S., M.A., M.U.F. and S.A.; data curation, M.S., M.A. and M.T.; writing—original draft preparation, M.S., M.A., M.T., M.U.F. and S.A.;

Declarations

Ethics approval Not applicable.

Informed consent Not applicable.

Conflict of interest The authors declare no competing interests.

References

1. Yoo SC, Kang B, Van Trinh P et al (2020) Enhanced mechanical and wear properties of Al6061 alloy nanocomposite reinforced by CNT-template-grown core–shell CNT/SiC nanotubes. Sci Rep 10:12896. https://doi.org/10.1038/s41598-020-69341-z

2. Samuel AU, Araoyinbo AO, Elewa RR, Biodun MB (2021) Effect of machining of aluminium alloys with emphasis on aluminium 6061 alloy – a review. IOP Conf Ser: Mater Sci Eng 1107:012157. https://doi.org/10.1088/1757-899X/1107/1/012157

3. Farooq MU (2023) Tribological characterization of a ball bearing subjected to an electric field: electric drivetrain tribology. (Dissertation). Retrieved from https://urn.kb.se/resolve?urn=urn:nbn:se:ltu:diva-100668

4. Farooq MU, Bhatti HA, Asad M et al (2022) Surface generation on titanium alloy through powder-mixed electric discharge machining with the focus on bioimplant applications. Int J Adv Manuf Technol 122:1395–1411. https://doi.org/10.1007/s00170-022-09927-1

5. Rafaqat M, Mufti NA, Ahmed N et al (2022) Hole-making in D2-grade steel tool by electric-discharge machining through non-conventional electrodes. Processes 10:1553. https://doi.org/10.3390/pr10081553

6. Akıncıoğlu S (2022) Taguchi optimization of multiple performance characteristics in the electrical discharge machining of the TIGR2. FU Mech Eng 20:237. https://doi.org/10.22190/FUME201230028A

7. Papazoglou EL, Karmiris-Obratański P, Leszczyńska-Madej B, Markopoulos AP (2021) A study on electrical discharge machining of titanium grade2 with experimental and theoretical analysis. Sci Rep 11:8971. https://doi.org/10.1038/s41598-021-88534-8

8. Farooq MU, Anwar S (2023) Investigations on the surface integrity of Ti6Al4V under modified dielectric(s)-based electric

9. Farooq MU, Anwar S, Hurairah A (2023) Reducing micro-machining errors during electric discharge machining of titanium alloy using nonionic liquids. Mater Manuf Process 0:1–16. https://doi.org/10.1080/10426914.2023.2236199

10. Asif N, Saleem MQ, Farooq MU (2023) Performance evaluation of surfactant mixed dielectric and process optimization for electrical discharge machining of titanium alloy Ti6Al4V. CIRP J Manuf Sci Technol 43:42–56. https://doi.org/10.1016/j.cirpj.2023.02.007

11. Mohije R, Titre H, Gohil V, Babruwan Meshram D (2023) A study in EDM electrode manufacturing using additive manufacturing. Mater Today: Proc. https://doi.org/10.1016/j.matpr.2023.01.044

12. Sari MM, Noordin MY, Brusa E (2012) Evaluating the electrical discharge machining (EDM) parameters with using carbon nanotubes. IOP Conf Ser: Mater Sci Eng 40:012019. https://doi.org/10.1088/1757-899X/40/1/012019

13. Dzulkifli NF, Mamat A, Choudhury IA (2020) The potential of water-in-oil emulsion of canola oil as dielectric fluid for EDM process. J Adv Res Fluid Mech Therm Sci 72:129–141. https://doi.org/10.37934/arfmts.72.2.129141

14. Muttamara A, Kanchanomai C (2016) Effect of carbon in the dielectric fluid and workpieces on the characteristics of recast layers machined by electrical discharge machining. Metall Mater Trans A 47:3248–3255. https://doi.org/10.1007/s11661-016-3452-4

15. Ming W, Xie Z, Cao C et al (2022) Research on EDM performance of renewable dielectrics under different electrodes for machining SKD11. Crystals 12:291. https://doi.org/10.3390/cryst12020291

16. Tönshoff HK, Egger R, Klocke F (1996) Environmental and safety aspects of electrophysical and electrochemical processes. CIRP Ann 45:553–568. https://doi.org/10.1016/S0007-8506(07)60510-1

17. Singh AK, Mahajan R, Tiwari A et al (2018) Effect of dielectric on electrical discharge machining: a review. IOP Conf Ser: Mater Scie Eng 377:012184. https://doi.org/10.1088/1757-899X/377/1/012184

18. Sivapirakasam SP, Mathew J, Surianarayanan M (2011) Constituent analysis of aerosol generated from die sinking electrical discharge machining process. Process Saf Environ Prot 89:141–150. https://doi.org/10.1016/j.psep.2010.10.003

19. Radu M-C, Tampu R, Nedeff V et al (2020) Experimental investigation of stability of vegetable oils used as dielectric fluids for electrical discharge machining. Processes 8:1187. https://doi.org/10.3390/pr8091187

20. Dhakar K, Kumar R, Katheria A et al (2022) Effect of various dielectric fluids on electric discharge machining (EDM): a review. J Braz Soc Mech Sci Eng 44:487. https://doi.org/10.1007/s40430-022-03778-3

21. Al-Amin M, Abdul Rani AM, Abdu Aliyu AA et al (2020) Powder mixed-EDM for potential biomedical applications: a critical review. Mater Manuf Process 35:1789–1811. https://doi.org/10.1080/10426914.2020.1779939

22. Talla G, Gangopadhayay S, Biswas C (2017) State of the art in powder-mixed electric discharge machining: a review. Proc Inst Mech Eng Part B: J Eng Manuf 231:2511–2526. https://doi.org/10.1177/0954405416634265

23. Baroi BK, Jagadish, Patowari PK (2023) Effect of boric acid in powder mixed EDM of Ti-6al-4V ELI. Mater Manuf Process 1–14. https://doi.org/10.1080/10426914.2023.2195907

24. Jampana VNR, Ramana Rao PSV, Sampathkumar A (2021) Experimental and thermal investigation on powder mixed EDM using FEM and artificial neural networks. Adv Mater Sci Eng 2021:1–12. https://doi.org/10.1155/2021/8138294

25. Sulakhe VN, Dalu R, Seth N et al (2018) Influence of powder-mixed dielectric on MRR and TWR in EDM process. In:

Proceedings of the 1st International Conference on Mechanical and Materials Science Engineering. AIP Conference Proceedings, Maharashtra, India, p 020021

26. Reddy VV, Valli PM, Kumar A, Reddy CS (2015) Multi-objective optimization of electrical discharge machining of PH17-4 stainless steel with surfactant-mixed and graphite powder–mixed dielectric using Taguchi-data envelopment analysis–based ranking method. Proc Inst Mech Eng Part B: J Eng Manuf 229:487–494. https://doi.org/10.1177/0954405414530904

27. Chaudhari R, Prajapati P, Khanna S et al (2022) Multi-response optimization of Al2O3 nanopowder-mixed wire electrical discharge machining process parameters of nitinol shape memory alloy. Materials 15:2018. https://doi.org/10.3390/ma15062018

28. Hosni NAJ, Lajis MA (2019) Multi-response optimization of the machining characteristics in electrical discharge machining (EDM) using span-20 surfactant and chromium (Cr) powder mixed. Materialwiss Werkstofftech 50:329–335. https://doi.org/10.1002/mawe.201800204

29. Abbas MA, Lajis MA, Abbas DR et al (2020) Influence of additive materials on the roughness of AISI D2 steel in electrical discharge machining (EDM) environment. Materialwiss Werkstofftech 51:719–724. https://doi.org/10.1002/mawe.201900243

30. Kolli M, Kumar A (2017) Surfactant and graphite powder–assisted electrical discharge machining of titanium alloy. Proc Inst Mech Eng Part B: J Eng Manuf 231:641–657. https://doi.org/10.1177/0954405415579019

31. Paswan K, Pramanik A, Chattopadhyaya S (2020) Machining performance of Inconel 718 using graphene nanofluid in EDM. Mater Manuf Process 35:33–42. https://doi.org/10.1080/10426914.2020.1711924

32. Rouniyar AK, Shandilya P (2021) Semi-empirical modeling and optimization of process parameters on overcut during MFAPM-EDM of Al6061 alloy. Pro Inst Mech Eng Part E: J Process Mech Eng 235:1784–1796. https://doi.org/10.1177/09544089211015890

33. Kumar S, Khedkar NK, Jagtap B, Singh TP (2017) The effects of cryogenic treatment on cutting tools. IOP Conf Ser: Mater Sci Eng 225:012104. https://doi.org/10.1088/1757-899X/225/1/012104

34. Harsha S, Dasharath SM (2021) Effect of cryogenic heat treatment & ageing on ultra fine grained aluminium–lithium alloy - a review. Mater Today: Proc 45:338–348. https://doi.org/10.1016/j.matpr.2020.10.1009

35. Dong N, Sun L, Ma H, Jin P (2021) Effects of cryogenic treatment on microstructures and mechanical properties of Mg-2Nd-4Zn alloy. Mater Lett 305:130699. https://doi.org/10.1016/j.matlet.2021.130699

36. Özdemir Z (2021) Shallow cryogenic treatment (SCT) effects on the mechanical properties of high Cr cast iron: low-carbon cast steel bimetallic casting. Inter Metalcast 15:952–961. https://doi.org/10.1007/s40962-020-00532-0

37. Senthilkumar D, Rajendran I (2011) Influence of shallow and deep cryogenic treatment on tribological behavior of En 19 steel. J Iron Steel Res Int 18:53–59. https://doi.org/10.1016/S1006-706X(12)60034-2

38. Choudhary R, Garg H, Prasad M, Kumar D (2017) Effect of cryogenic treatment of tool electrode on the machining performance and surface finish during electrical discharge machining of Hastelloy C-4. Mater Today: Proc 4:1158–1166. https://doi.org/10.1016/j.matpr.2017.01.132

39. Thanigaivelan R, Arunachalam R, Natarajan N (2015) Study on influence of electrodes in electric discharge machining. MENG 8:161–167. https://doi.org/10.2174/2212797608666150610220531

40. Teimouri R, Baseri H (2012) Study of tool wear and overcut in EDM process with rotary tool and magnetic field. Adv Tribol 2012:1–8. https://doi.org/10.1155/2012/895918

41. Kumar A, Sharma R (2020) Multi-response optimization of magnetic field assisted EDM through desirability function using response surface methodology. J Mech Behav Mater 29:19–35. https://doi.org/10.1515/jmbm-2020-0003

42. Rashedul IMd, Zhang Y, Zhou K et al (2021) Influence of different tool electrode materials on electrochemical discharge machining performances. Micromachines 12:1077. https://doi.org/10.3390/mi12091077

43. Meena VK, Azad MS, Singh S, Singh N (2017) Micro-EDM multiple parameter optimization for Cp titanium. Int J Adv Manuf Technol 89:897–904. https://doi.org/10.1007/s00170-016-9130-2

44. Ramaswamy A, Perumal AV (2020) Multi-objective optimization of drilling EDM process parameters of LM13 Al alloy–10ZrB2–5TiC hybrid composite using RSM. J Braz Soc Mech Sci Eng 42:432. https://doi.org/10.1007/s40430-020-02518-9

45. Athul S, Premnath G, Sunil B, Rajeev VR (2018) Elevated temperature wear behavior of aluminium alloy (Al 6061). National Conference on Latest Trends in Mechanical Engineering NCLTME, Palakkad, Kerala, India

46. Kassem MGA, Ahmed A-MM, Abdel-Rahman HH, Moustafa AHE (2019) Use of Span 80 and Tween 80 for blending gasoline and alcohol in spark ignition engines. Energy Rep 5:221–230. https://doi.org/10.1016/j.egyr.2019.01.009

47. Mohanty CP, Satpathy MP, Mahapatra SS, Singh MR (2018) Optimization of cryo-treated EDM variables using TOPSIS-based TLBO algorithm. Sādhanā 43:51. https://doi.org/10.1007/s12046-018-0829-7

48. Hasçalık A, Çaydaş U (2007) Electrical discharge machining of titanium alloy (Ti–6Al–4V). Appl Surf Sci 253:9007–9016. https://doi.org/10.1016/j.apsusc.2007.05.031

49. Nas E, Akıncıoğlu S (2019) Optimization of cryogenic treated nickel-based superalloy in terms of electro erosion processing performance. Acad Platform J Eng Sci 7:115–126

50. Srivastava V, Pandey PM (2012) Performance evaluation of electrical discharge machining (EDM) process using cryogenically cooled electrode. Mater Manuf Process 27:683–688. https://doi.org/10.1080/10426914.2011.602790

51. Prakash C, Singh S, Singh M et al (2018) Multi-objective particle swarm optimization of EDM parameters to deposit HA-coating on biodegradable Mg-alloy. Vacuum 158:180–190. https://doi.org/10.1016/j.vacuum.2018.09.050

52. Shrivastava P, Paul B, Fuskele V (2021) AI based modeling of quality parameter in EDM using advanced material for energy optimization. SSRN Journal. https://doi.org/10.2139/ssrn.3950151

53. Moré JJ (1978) The Levenberg-Marquardt algorithm: implementation and theory. In: Watson GA (ed) Numerical analysis. Springer, Berlin Heidelberg, Berlin, Heidelberg, pp 105–116

54. Sana M, Farooq MU, Anwar S, Haber R (2023) Predictive modelling framework on the basis of artificial neural network: a case of nano-powder mixed electric discharge machining. Heliyon e22508. https://doi.org/10.1016/j.heliyon.2023.e22508

55. Suvarna M, Jahirul MI, Aaron-Yeap WH et al (2022) Predicting biodiesel properties and its optimal fatty acid profile via explainable machine learning. Renew Energy 189:245–258. https://doi.org/10.1016/j.renene.2022.02.124

56. Bains PS, Mahajan R, Sidhu SS, Kaur S (2019) Experimental investigation of abrasive assisted hybrid EDM of Ti-6Al-4V. J Micromanufac 2:123–132. https://doi.org/10.1177/2516598419833498

57. Perumal A, Azhagurajan A, Prithivirajan R, Kumar SS (2021) Experimental investigation and optimization of process parameters in Ti – (6242) alpha–beta alloy using electrical discharge machining. J Inorg Organomet Polym 31:1787–1800. https://doi.org/10.1007/s10904-020-01786-1

58. Choudhary R, Kumar A, Yadav G et al (2020) Analysis of cryogenic tool wear during electrical discharge machining of titanium alloy grade 5. Mater Today: Proc 26:864–870. https://doi.org/10.1016/j.matpr.2020.01.080